Rev 2

The electron excitation function of H Lyman-α from threshold to 1.8 keV

G. K. James
Jet Propulsion Laboratory
California Institute of Technology
Pasadena, California 91109

J. A. Slevin
Department of Experimental Physics
St. Patrick's College, Maynooth
Co. Kildare, Ireland

D. E. Shemansky
Department of Aerospace Engineering
University of Southern California
Los Angeles, California 90089

J. W. McConkey
Department of Physics
University of Windsor
Windsor, Ontario N9B 3P4, Canada

D. Dziczek
Institute of Physics
Nicholas Copernicus University
Torun, Poland

I. Kanik and J. M. Ajello
Jet Propulsion Laboratory
California Institute of Technology
Pasadena, California 91109
(July 17, 1996)

A ostrac

The excitation function of prompt Lyman-α radiation, produced by electron impact excitation of atomic hydrogen, has been measured for the first time over an extended energy range from threshold to 1.8 keV. Measurements were obtained in a crossed-beams experiment using both magnetically confined and electrostatically focused electrons in collision with atomic hydrogen produced by an intense discharge source. A vacuum ultraviolet (VUV) monochromator system was used to measure the emitted Lyman- α radiation. The absolute H (1s – 2p) cross section was obtained from the experimental excitation function by normalizing to the accepted optical oscillator strength, with corrections for polarization and cascade. Our data are significantly different from the earlier experimental results of Long et al. [1] and Williams [2,3], which were limited to energies below 200 eV. The measured excitation function shows excellent agreement in shape with recent theoretical convergent close coupling (CCC) calculations over a two order of magnitude range in energy. Statistical and known systematic uncertainties in our data range from ± 4% near threshold to ± 2% at 1 keV. Multistate coupling affecting the excitation function to 1 keV is apparent in both the present experimental and recent theoretical results. This shape function effect leads to an uncertainty in absolute cross section at the 10% level in the analysis of our experimental data. The derived absolute cross section is within 7% of the recent CCC calculations over the eV .8 keV range of .he experimen

34.80. Dp 39.10.+ j, 31.15.+p 33.20.Ni

I. INTRODUCTION

Atomic hydrogen has been of continuous experimental and theoretical interest for well over half a century. Experimental measurements of its line spectrum have provided searching tests for Quantum Electrodynamics. Hydrogen has played a central role in atomic collision physics, primarily because hydrogen wavefunctions are exact and a precise description of the hydrogen target is available for modeling the collision process. Atomic hydrogen, the most abundant species, is also of great cosmological interest.

Excitation of atomic hydrogen by electron impact has been a key testing ground for the development of the theory of electron impact excitation. However, as pointed out in recent reviews by Trajmar and Kanik [4] and King et al. [5], significant discrepancies still remain between available experiments, as well as between experiment and theory. To a large extent this reflects the difficulty in performing experiments with atomic hydrogen, where stable, intense and well quantified beams of the atomic species are difficult to produce. It also reflects the difficulties experienced by theorists in the so called 'intermediate' energy region, away from the threshold region, where high energy approximations are also not valid.

The first measurement of the H(1s – 2p) excitation cross section (Q_{1s2p}) was [illegible] out almost 40 years ago by Fite and Brackman [6] in a pioneering experiment using a tungsten furnace to dissociate molecular hydrogen and an oxygen filter to isolate the Lyman-α radiation. In 1968 Long, Cox and Smith [1] carried out a similar study, also using a tungsten furnace and oxygen filter, and normalized their data to the Born approximation at an energy of 200 eV. These data correspond to observations of Lyman-α radiation at 90° to the interacting beams and require a correction for the effect of polarization in order to obtain full integral cross sections. McGowan, Williams and Curley [7] published measurements of the H(1s – 2p) cross section in the threshold region primarily to observe the resonance structure. Finally, Williams [2,3] reported absolute Q_{1s2p} cross section [illegible] for energies between threshold and 13 eV, and for a single energy at 54.4 eV, calibrating the radiometric system in terms of the quantum yield of a freshly evaporated aluminum film and using a phase shift analysis of the elastic scattering to determine the target hydrogen density.

Because of an extended energy range, the data of Long et al. [1] have [illegible] of greatest interest and the subject of much analysis by different authors. van Wyngaarden and Walters [8] corrected the Long et al. [1] data at all energies using Ott, Kaupila and Fite's [9] values of polarization and Morrison and Rudge's [10] estimates of cascade from higher lying levels up to n = 5. van Wyngaarden and Walters [8] then normalized the data by scaling the resulting experimental value to their theoretical value at 200 eV. [illegible] and Gallagher [11] considered the normalization of the Long et al. data [1] by correcting for cascade at higher energies using the Born coefficients of Vainshtein [12] and by developing a procedure to extrapolate the experimental data to a Bethe Fano [13] plot. They [illegible] corrected values and suggested that these [illegible] represent an upper limit to the true cross section, because of the remaining uncertainty in convergence to the Born high energy dependence. Madison [14] also discussed theoretical evidence suggesting that the [illegible] data should be reduced by approximately 5% because of the inadequacy of the Born approximation at 200 eV where their data were initially normalized. All of these analyses have led to various 'corrected' forms of the [illegible] data of Long et al. [1]. Thus, at the theoretically interesting energy of 54.4 eV,

the Long et al. *[1]* value for Q_{1s2p} (interpolated from their data at 48.6 eV and 68.6 eV) is quoted as 0.708 au (van Wyngaarden and Walters [8] and 0.789 au (Hall and Gallagher [11]). Error bars in the original Ref. [1] values for Q_{1s2p} near 54.4 eV are stated as ±4%.

Comparison of the absolute measurements of Williams [2,3] and the cross sections of Long et al. [1], shows that at 54.4 eV the cross section datum of Williams (Q_{1s2p} = 0.888 ± 0.076 au) lies significantly higher (from 13% to 25%) than any of the corrected Long et al. [1] values. While in the context of experimental collision physics this may not seem a large divergence, given the combined error bars on the two measurements, this discrepancy is nevertheless viewed as significant, in part because the measurement of excitation functions of atomic hydrogen has fundamental importance for the development of theoretical models, and also in part because of the importance of the (1S – 2p) Lyman-α cross sections for H and H_2 in providing secondary standards for absolute radiometric calibration (van der Burgt et al. [15], Shemansky et al. [16]).

The discrepancy between the data of Long et al. [1] and Williams [2,3] has provoked a sustained debate in the literature. The extensive calculations over the last few decades for excitation of atomic hydrogen have been compiled in the recent comprehensive review of Trajmar and Kanik [4] and will not be repeated here. There are two fundamental approaches to the electron scattering problem: a perturbative approach which is generally accurate at high energies and extends down to the intermediate region (the various Distorted Wave Born Approximations (DWBA2) of Madison and co-workers (Madison [14], Bubelev et al. [17]) are examples of this approach); a non-perturbative approach, based on an expansion of the scattering wavefunction in terms of a suitable set of basis states (the R-matrix approach of Burke and co-workers (Burke et al. [18]) and various close-coupling calculations are examples). The most accurate theoretical data in the intermediate energy range are likely to be the non-perturbative convergent close coupling calculations (CCC) of Bray and Stelbovics [19] and Bray [20], whose results lie significantly below the Williams datum at 54.4 eV but also above the Long et al. [1] data scaled by Ref. [8]. These CCC calculations are supported in varying degrees by the multi-pseudostate calculations of Callaway and Unnikrishnan [21], van Wyngaarden and Walters [8,22], Scott et al. [23], the second-order distorted wave Born approximation (DWBA 2) calculations of Kingston and Walters [24], and Bubelev et al. [17], and the unitarized eikonal Born series (UEBS) calculations of Byron et al. [25], as shown in Figure 1.

In order to resolve these outstanding discrepancies between the few available experiments, and between experiment and theory, we report here a comprehensive measurement of the prompt H Lyman-α excitation function from threshold to 1.8 keV. The present experimental data correspond to observations of the Lyman-α signal at an angle of 90° to the incident electron beam direction and have to be corrected for polarization of the radiation, as well as cascade from higher states.

Several aspects of our measurements are significant:

1. The extension of the excitation function measurements up to an energy of 1.8 keV allows a significantly better approach to the dominance of the zero order term in the first Born approximation.

2. The present experimental approach uses a modern, efficient source of atomic hydrogen capable of producing atom densities three orders of magnitude greater than those used

in the earlier experimental work,

3. In contrast to previous work, where an oxygen filter was used to isolate the Lyman-α line, a VUV spectrometer is used for wavelength selection. This not only accurately isolates the Lyman-α emission, but also greatly increases the accuracy of the determination of the molecular contribution to the observed photon signal.

4. We have used a stable, high efficiency Lyman-α detector based on a CsI coated channeltron with a quantum efficiency of 15% for 121.6 nm radiation

II. APPROACH AND THEORETICAL BACKGROUND

The determination of integrated cross sections for optically allowed transitions from observations of the radiation emitted at either 90° or at the 'magic angle' 54.7° with respect to the incident electron beam direction has a long and well established history (Heddle and Gallagher [1 1], van der Burgt et al. [15], Filipelli et al. [26]). Here we provide a brief description of the method.

A beam of hydrogen atoms, effusing from a radio frequency (rf) dissociator, is crossed by a beam of electrons of variable energy and observations are made on the Lyman-α emission at 90° using a vacuum monochromator for wavelength selection. At sufficiently low pressures, where radiationless deactivation and self-absorption effects can be neglected, we write a simple relationship relating the rate of photon emission, I_{ji}, in a transition from a state j to a final state i as

$$I_{ji} = i_e n_i \ell Q_j \tag{1}$$

where i_e is the electron beam current in electrons per second, n_i is the number density of the target gas, ℓ is the path length of the electron beam through the target, and Q_j is the total cross section for the excitation process. Thus an absolute measurement of the intensity, I_{ji}, radiated in all directions, gives the integrated cross section provided the other experimental parameters in Eq. 1 are known. In general the upper level j is populated indirectly by radiative cascade, as well as directly from state i. Thus to obtain the true total cross sections for excitation from the ground state, it is necessary to make corrections for cascade transitions.

The rate of photon emission at an angle θ to the electron beam is given by

$$I_{ji}(\theta) = \frac{I_{ji}}{4\pi}\left[1 - \frac{P}{2}\cos^2\theta\right] \tag{2}$$

where P is the polarization of the emitted radiation and characterizes the anisotropy of the emission process. The present experimental geometry involves observations at 90°. Therefore, we obtain

$$I_{ji} = 4\pi I_{ji}(90°)(1 - P/3) \tag{3}$$

A measurement of $I_{ji}(90°)$ yields an apparent cross section $Q_j(90°)$ which must be corrected to obtain the true integrated cross section.

It is not possible to determine all the factors in (1) absolutely, requiring a suitable normalization procedure in order to place the relative measurements on an absolute scale. One of the most widely used techniques for this purpose is to normalize the data to the Born approximation at sufficiently high energy where its validity is assumed while ensuring that the electron and atom beam overlap does not vary significantly as the incident electron energy is ramped from higher to lower energies. Two different techniques using this basic approach are presented in the analysis of present experiment. A conventional normalization procedure using a Bethe-Fano plot was applied in the manner described by Heddle and Gallagher [11] in which the experimental data is scaled to approach the asymptotic limit at high energy defined by the Bethe-Fano line. The slope and intercept of this Bethe-Fano line are defined for an uncoupled (1s 2p) system. A normalization procedure using a one-parameter analytic fitting function which is sensitive to the subtle effects of any multistate coupling is also presented. The limiting factor in obtaining high accuracy in cross section measurement in this case is the influence of multistate coupling which extends to unusually high energy (~ 1 keV for the 1 (1s 2p) excitation process.

A. Analytic Methods

The first Born approximation for electric dipole excitation is described by Mott and Massey [27] in the form of the momentum transfer integral,

$$Q_{ij} = \frac{4\pi a_o^2 z^2}{E} \int_{\zeta_{min}}^{\zeta_{max}} \frac{f_{ij}(K)d\zeta}{E_{ij}\zeta} \tag{4a}$$

$$\zeta = (K a_o)^2 \tag{4b}$$

$$\Omega_{ij} = \omega_i E \frac{Q_{ij}}{\pi a_o^2 z^2} \tag{4c}$$

$$\Omega_{ij} = 4\omega_i \int_{\zeta_{min}}^{\zeta_{max}} \frac{f_{ij}(K)d\zeta}{E_{ij}\zeta} \tag{4d}$$

where a_o is the Bohr radius, z, nuclear charge of the target, E, energy of the impacting particle in Rydbergs, $f_{ij}(K)$, generalized oscillator strength for transition from state i to state j, K is the momentum transfer magnitude, and ω_i is the lower state degeneracy. A more convenient working relationship is used in equations 4c and 4d in which the momentum transfer integral is related to the fundamental collision strength quantity, Ω.

The range of ζ is given by the relations

$$\zeta_{max} = 2E\left(\frac{\mu}{m}\right)^2 \left\{1 - \frac{1}{2}\frac{m}{\mu}\frac{1}{X} + \left[1 - \frac{m}{\mu}\frac{1}{X}\right]^{\frac{1}{2}}\right\} \tag{5a}$$

$$X = \frac{E}{E_{ij}} \tag{5b}$$

$$\zeta_{min} = 2E\left(\frac{\mu}{m}\right)^2 \left\{1 - \frac{1}{2}\frac{m}{\mu}\frac{1}{X} - \left[1 - \frac{m}{\mu}\frac{1}{X}\right]^{\frac{1}{2}}\right\} \tag{5c}$$

where μ is the reduced mass of the collision complex, and m is the mass of the impactor. If the impacting particle is an electron the relationships reduce to

$$\zeta_{max} = 2E_{ij}X\left[2 - \frac{1}{X} - \frac{1}{8}\frac{1}{X^2} - \cdots\right] \tag{6a}$$

$$\zeta_{min} = \frac{1}{4}\frac{E_{ij}}{X}\left[1 + \frac{1}{2}\frac{1}{X} + \frac{5}{16}\frac{1}{X^2} + \cdots\right] \tag{6b}$$

Contrary to the statement by Inokuti [28], both limits must be applied to the integral in order to obtain an accurate derivation of the Born approximation (Ref. [29]). For the 11 (1s 2p) transition, the generalized oscillator strength is given by [27]

$$f_{12}(K) \quad E_{12} \cdot 2^{15} \cdot 3^{-10}(1 - \frac{4}{9}\zeta)^6 \tag{7}$$

The substitution of (7) into (4d) reduces to

$$\Omega_{12} = C_7 \int_{\zeta_{min}}^{\zeta_{max}} \frac{d\zeta}{\zeta\left(1 + \frac{4}{9}\zeta\right)^6} \tag{8a}$$

$$C_7 = 4\omega_1 M_{12}^2 \tag{8b}$$

$$M_{ij}^2 = \frac{f_{ij}}{E_{ij}} \tag{8c}$$

$$\Omega_{12} = C_7\left[ln\left(\frac{\zeta}{1 + \frac{4}{9}\zeta}\right) + \sum_{i=1}^{5}\frac{1}{i}\frac{1}{(1 + \frac{4}{9}\zeta)^i}\right]_{\zeta_{min}}^{\zeta_{max}} \tag{8d}$$

where M_{ij} is the dipole matrix element. The relation 8d differs from the equivalent equation (4.6) given in Inokuti [28]. In approximation, (8d) reduces to

$$\Omega_{12} = C_5 + \frac{C_6}{X} + C_7 ln(X) \tag{9a}$$

$$C_5/C_7 \quad 0.2021 \tag{9b}$$

$$C_6/C_7 = 0.7501 \tag{9c}$$

$$C_7 = 4.447 \tag{9d}$$

The normalization procedure described in detail by 11('(1(11(' and Gallagher [11] essentially forces the experimental collision strength data (plotted against log(E)) to approach a Bethe-Fano line asymptotically at high energy. The formulation for this Bethe-Fano line is equivalent to relation 9a but without the C_6 term. The slope (determined from the constant C_7) is related to the accepted optical oscillator strength and the energy intercept is fixed using the Born value of C_5 for an 1111('011])1('(1 system. In an alternative normalization approach, a modified Born analytic function is used [1 6,3 0] to fit the collision strength curve over the entire range of energy. This is given by the equation

$$\Omega = \frac{C_0}{X^2} + \sum_{i=1}^{4} C_i \cdot exp(-i \cdot C_8 \cdot X) + C_5 + \frac{C_6}{X} + C_7 ln(X) \tag{lo}$$

where the additional terms with constants C_0, C_4, C_8, represent correlation exchange and configuration mixing contributions to the total collision strength. A resonance component at threshold [2] is not included in (10), but is treated in a following paper [31]. The analytic fitting technique has advantages over the conventional Bethe-Fano procedure: 1) It provides a measure of the magnitude of the deviation from the Born approximation at high energies caused by the influence of multistate coupling, and 2) The best fit function utilizes the entire energy range determining the shape function of the experimental data.

Analysis, using equation (10), of the recent CCC calculations of [17] and the modification of these results by Bray [20] lead to a range of values of the coefficients depending on the high energy truncation of the data set. This variation as discussed further below is an indicator both of the heavy correlation of terms and limitation in accuracy of the CCC calculations at the few percent level. This fact sets a fundamental limit on the ability to obtain independent accurate experimental measurements of the H (1s - 2p) cross section through analysis of the shape function in spite of the extension of the measurements to 1,8 keV.

The generalized oscillator strength (7) is based on the uncoupled properties of the 1s 2p configuration. As we show below, the 1s - 2p excitation function both experimentally and theoretically has the characteristics of a heavily coupled system that extends over a broad impact energy range, indicating substantial deviation from the shape of (7). The terms in (9a) that depend on the shape of the generalized oscillator strength, C_5 and C_6, therefore should not be regarded as accurate quantities. There is no indication that the optical oscillator strength calculated from the Coulomb approximation (Ref. [32]) is measurably affected by coupling, and we assume that the value of C_7 is accurately determined by Eq. (9).

III. EXPERIMENT

A. Apparatus

The experimental apparatus is shown schematically in Figure 2. It consists of an electron impact chamber equipped with an atomic hydrogen source, in tandem with a 0.2 meter VUV monochromator (resolving power 250) and CsI-coated channeltron detector positioned after the exit slit of the monochromator. Two very different electron guns have been used in the present experiment: a relatively simple 3 element gun which uses magnetic field confinement and a 6 element electrostatic gun, designed and constructed by Kimball Physics, Inc [*]. The magnetic gun, shown in Figure 2, was used for low energy measurements, while the electrostatic gun (Figure 3) was used for the higher energies. The use of two different gun designs is crucial to the success of the present experiment. To achieve the correct normalization, it is essential to measure the very weak signals at high energies to high accuracy. Since the confining magnetic field traps secondary electrons from ionization processes, and further since the magnetic gun design is such that a small number of low energy secondaries are inevitably produced from collisions at high energies with the gun apertures, it is essentially impossible to reach the Born limit at high energies with a magnetic gun. Thus, a well designed electrostatic gun is essential for the high energy measurements. On the other hand, it is difficult to maintain a constant beam cross section down to the lowest energies using an electrostatic gun, and the experimental signal is sensitive in the present

experiment to any change in the electron beam/atom beam overlap. Variations in the size of the electron beam are essentially removed by the use of magnetic field confinement.

The magnetic electron gun and monochromator systems have been described in detail in earlier publications [33,34]. Thermionic electrons produced by heating a tungsten filament are extracted by a Pierce electrode and extractor lens combination and accelerated or decelerated by an aperture lens (or anode) to achieve the final energy. The electron beam is collimated by the axially symmetric magnetic field (60 Gauss) produced by a quadrupole solenoid arrangement. Ramping of the electron beam energy is controlled by a multichannel analyzer (MCA), and the data are accumulated in the MCA memory.

The electrostatic gun was custom designed as a complete subsystem by Kimball Physics, Inc. and uses a unipotential refractory metal cathode to produce a beam of low energy spread (~0.3 eV). By use of multistaging and a computer-designed zoom lens, a constant focal plane position is maintained over the energy range from 10 eV to 2.0 keV, with a constant spot size (~1.3mm diameter) in the range 50-1800 eV. The direction of the output beam can be controlled by a set of X and Y deflectors. Currents of ~5 μA are typical at all energies. Programmable power supplies provide voltages for all of the gun elements. The entire gun operation is controlled by a PC operating in a Lab Windows [i] environment.

A deep Faraday cup (aspect ratio ~10:1), designed to eliminate back scattered secondary electrons, is used to collect and monitor the electron beam current. The rear surface of the inner Faraday Cup is electrically isolated from the outer cylinder and is coated with) carbon soot." By suitable biasing (typically the inner cup is at +60 volts and the outer cylinder at +10 volts), more than 99% of all the current appears in the inner Faraday Cup at all energies, the remainder being collected on the outer cylinder. Measurements of the Lyman-α signal were carried out for a large range of bias voltages and electron energies to ensure that any field penetration of Cup voltages into the interaction region did not lead to quenching of metastable atoms within the field of view of the detection system. No effect was observed, indicating that field penetration from the Faraday Cup was not a significant effect.

The atomic hydrogen source has been described in detail by Slevin and Sterling [35] and is shown in Figure 4. Hydrogen molecules are dissociated in a discharge, excited within an rf cavity, resonant at 36 MHz. Hydrogen atoms effuse from the water cooled Pyrex discharge tube, past a VUV photon trap and through a 1mm capillary into a field-free interaction region where they are crossed with the electron beam. Photons emitted from the interaction region and orthogonal to the electron and atom beams are wavelength selected by a VUV monochromator with slit widths chosen to ensure adequate separation of atomic line emissions. This radiation is detected by a channeltron, coated with a suitable CsI layer to enhance quantum efficiency at 121.6 nm The effectiveness of the photon trap in preventing stray photons, generated within the discharge tube, from being detected was verified by measuring the spectrum produced in the absence of the exciting electron beam. No measurable Lyman-α radiation was detected under these conditions.

The VUV monochromator system is rotated such that the plane defined by the monochromator entrance slit and optic axis is at 45° to the electron beam axis (see Figure 5). This orientation removes polarization effects that may be induced by the monochromator and detector systems, as described by Clout and Heddle [36] and Donaldson et al. [37].

Precise wavelength selection, using the VUV monochromator, is a critical factor in quantifying the molecular contribution to the observed Lyman-α signal. The use of an oxygen

filter in the previous work of Long et al. [1] and Williams [2,3] introduces uncertainty as to precisely what spectrum is transmitted to the detector. An oxygen filter has a transmission window that spans several molecular emissions. It is difficult in practice to accurately estimate the molecular content in the observed signal when an oxygen filter is used, due to the unavailability of accurate absorption data for the high pressures at which these filters are used. This uncertainty contributed to the large systematic error found for the dissociative cross section for Lyman-α from H_2 used as a calibration standard for many years [16]. The use of a monochromator will enable future measurements to be made with this apparatus of the excitation functions of other members of the Lyman series.

The entire experimental system is interfaced to a PC which monitors all important experimental parameters and controls the electron beam energy in the case of the electrostatic gun. Measured signals are normalized to the electron beam current and hydrogen source pressure (measured by a very stable and accurate Varian Model CHMX-11-001 capacitance manometer), eliminating variations in these quantities as sources of systematic error. Data are accumulated in a multiple scanning mode to reduce the effects of drift in other experimental parameters.

B. Correction procedure for polarization

Lyman-α signals measured at 90° are corrected for polarization in the manner described in Sec. II in order to obtain values for the total cross section. In the region from threshold to 200 eV, the values for polarization measured by Ott et al. [9] were used to correct our experimental data. At energies above 200 eV, the polarization calculations of McFarlane [38] were used. Ref. [38] employed a Born procedure to find values for polarization P which are represented by the formula

$$P = \frac{P_0\left[3 - \ln\left(\frac{E}{E_0}\right)\right]}{(2 - P_0)\ln\left(\frac{E}{E_0}\right) + P_0} \tag{11}$$

where $E_0 = 8.337$ eV and $P_0 = 0.42$, is the polarization parameter [39].

We use the above dichotomy, in spite of the availability of data from Ott et al. [9] above 200 eV, because the Ott data have relatively large errors in this region and we believe the McFarlane data are more reliable. However, it should be emphasized that whatever approach is taken to this polarization correction, the correction itself is not large, ranging from a maximum of 8% at low energies to 3% at the highest energies.

C. Correction procedure for molecular emission contamination

Since the hydrogen beam is not fully dissociated, the observed photon signal at Lyman-α, obtained with the rf discharge, contains a contribution from molecular emission which must be quantified and subtracted in order to obtain the net (eq. 11) excitation function. The molecular component results from Lyman-α radiation produced by dissociative excitation of the molecule, as well as radiation from molecular bands transmitted by the bandpass of the monochromator (FWHM 2.4 nm at typical slit widths of 600 μm). In order to correct the

measured excitation function for this molecular contribution, the dissociation fraction must be measured, together with the corresponding excitation function with the discharge off.

The dissociation fraction is established in the manner described by Forand et al. [40] by tuning the monochromator to an H_2 molecular band at 110.0 nm (with the bandpass adjusted to exclude any atomic component from Lyman-α or Lyman-β) and measuring the molecular emission with the discharge on and off at the same hydrogen source driving pressure and beam current. The dissociation fraction D is the ratio of atoms to the total number of particles in the beam and is related to these two signals S_1 (discharge on) and S_2 (discharge) by the relationship

$$D = 2 \left(\frac{T_2}{T_1}\right)^{\frac{1}{2}} \frac{S_1}{S_2} \tag{12}$$

where T_1 and T_2 are the effective kinetic temperatures in the gas beam with the discharge on and off, respectively. Woolsey et al. [41] and Forand et al. [40] measured these kinetic temperatures in an identical source and found that the two temperatures were equal, confirming the reasonable assumption that the source indeed thermalizes the hydrogen beam.

Once the dissociation fraction has been established, the net (e+H) Lyman-α signal S_H can be obtained from measurements of S_1 and S_2 made at Lyman-α with the discharge on and off, respectively, using the relationship derived by [40]

$$S_H = S_1 - (1 - D) S_2 \tag{13}$$

This correction procedure is applied at each electron impact energy by measuring excitation functions under the same conditions with the discharge on and off.

Typical VUV emission spectra produced by electron impact at 100 eV with the RF discharge on and off are shown in Figure 6 at a spectral resolution of 5 nm (FWHM). The same molecular subtraction procedure used for the excitation function data can be applied to these spectra, yielding the net (e+H) spectrum also shown in Figure 6. Lyman series members up to $n = 6$ can be clearly identified in our net (e+H) spectrum, together with the series limit at 91.113 nm. The molecular bands around 110.0 nm used in the determination of the dissociation fraction can be seen in the spectrum of the undissociated molecular beam. A typical value for the measured dissociation fraction is 0.65 ± 0.02.

D. Resonance trapping

Since the H(2p) excited state connects radiatively with the ground state, it is critical to ensure that the excitation function measurements are free from resonance radiation trapping effects. Operating under Knudsen conditions at the beam source preserves a linear relationship between the source pressure and the number density in the interaction region. Figure 7 illustrates the relationship between the source pressure (measured by the Varian capacitance manometer) and the Lyman-α signal detected at 100 eV. These data verify the absence of resonance radiation trapping for source pressures less than 46 m'Torr, where the detected photon signal is proportional to the hydrogen source pressure. All of the measurements reported here were obtained at hydrogen pressures of $\sim$ 40 m'Torr.

E. Cascade correction

The observed Lyman-α photon signal includes a contribution from the decay of higher lying states cascading into the 2p level. This has been calculated using an atomic hydrogen model constructed to the $n = 9$ level, with a collisional radiative equilibrium code [412,31], which establishes the emission line intensities for the entire system to a selected principal quantum number upper limit, providing an exact calculation of the cascade contribution for the given cross sections. Cross sections in the model for the np orbitals have been calculated by scaling the $(1s \rightarrow 2p)$ cross section obtained by Bray [20], according to the oscillator strength of the transition. Excitation cross sections to the ns and nd levels have also been derived from Bray [20]. The cascade contribution has been established as an analytic function using (10) with coefficients given in Table 1.

The cascade contribution calculated here has been compared to the calculated cascade corrections based on the Morrison and Rudge [10] formulation for levels up to $n = 5$, using the CCC calculations of Ref. [?,()], with excellent agreement.

Figure 8 shows the integrated cascade cross section feeding the H(2p) state, calculated by Ref. [31], and the correction to the measured H $(1s \rightarrow 2p)$ collision strength. The experimental data shown in Figure 8 has been corrected for the effect of polarization and normalized using the analytic fitting procedure described in Sec. IV. The cascade correction to the $(1s \rightarrow 2p)$ cross section is significant near threshold. At energies below 20 eV the correction is in excess of 15% and at 14 eV the contribution is 5%.

It is important to ensure that the calculated cascade fractions are applicable to our particular experimental configuration. It has been pointed out by van Zyl and Gealy [43] that very small electric fields can greatly perturb calculated cascade fractions. The precautions, indicated earlier, taken to exclude stray fields from the interaction region to prevent quenching of H(2s), should also ensure that perturbing effects of this type are not present in our experiment. These factors are discussed in detail in the Appendix.

A further effect which must be considered when using the magnetically collimated gun is the motional electric field experienced by the moving atoms in the magnetic field. This effect has been considered by van Zyl et al. [44]. They show that motional fields as low as 1 V/cm can have significant state-mixing effects with a consequent impact on the decay channels, particularly for $n > 4$. For atomic hydrogen atoms of 50 meV energy, a motional electric filed of ~ 0.3 V/cm is estimated at a field B = 100" G. Calculations show that if fields of 1 V/cm are assumed, the cascade contribution will be reduced by at most 5%. van Zyl et al. [44] also comment on the fact that Zeeman splitting of the levels in a magnetic field could affect the branching ratios for the decay. They suggested that this effect should be small [o]" fields less than a few gauss. Since this effect would be most pronounced for the higher n levels, when the cross sections are very small, we anticipate that at the fields used in the present experiment a negligible effect on the cascade contribution will occur.

All of the above assumes that the cascade radiation is unpolarized. The main contribution to any polarization of the cascade radiation comes from the nd states where the radiation is normally very weakly polarized. The overall effect of polarization of the cascade radiation is therefore expected to be very small, less than 1% in the worst case at low energies.

We note that the dwell time of atoms in the field of view of the spectrometer is about 2 μsec. This eliminates excited atoms in states above $n = 8$ as contributors to cascade into

the H(2p) state.

IV. AN ALYSIS OF I) ATA

A. Experimental data

As described in Sec. 111, the experimental data was obtained in two groups using different electron gun designs. The lower energy region was explored using the magnetically collimated gun to an 11))])('1" limit in energy of 200" eV. Beyond 200 (eV to the peak beam energy of I .8 keV the relative cross sections were obtained using the electrostatic electron gun. The combined statistical and known systematic uncertainties in the measurements have been estimated 10 range from 4% at energies near till"('s1)o1(1 to 2% at 1 .8 H(\'. The details of the error analysis are provided in the Appendix. The electron beam energies were established in absolute value at low energy by using the sharp threshold for the dissocexcitation of the Lyman-α line as a benchmark. The fact that the measurements were on a relative scale, required the establishment of a normalization procedure for merging the low and high energy region data sets into a single data volume for analysis. The validity of matching the magnetic and electrostatic data at ~ 200 eV has been confirmed, in a separate experiment, by measuring the Lyman-α signal (normalized to electron beam current and hydrogen source pressure) at 200 eV as a function of a magnetic field, applied collinearly with the (lee/7Yj.$lotic *gun*, using the same quadrupole magnet configuration employed for the magnetic gun. At field strengths of (), '20> 40 and 60 Gauss, no statistically significant change in the normalized signal was observed, confirming the absence of any beam overlap problems at the ('11('1"{',)' where the two data sets were III('I"/$'(I.

The data sets were merged by minimizing the root mean square error of the analytic fitting process in the energy region surrounding 200 eV, after the previous corrections for polarization and cascade effects were applied on a relative basis as a (correction k) the shape function. The fitting process was accomplished using an iterative calculation that established the constant terms in Eq 10. Figure 9 shows the combined data plotted as collision strength compared to the derived analytic function. The combined experimental data after corrections described above for cascade and polarization are listed in Table 11, and compared with the values obtained from the analytic fit using Eq. 10. The experimental data were placed on an absolute scale determined by fixing the value of C_7 by the kilo\\'li absorption oscillator strength (see Ref. [45], Eq. 9d). The higher order constants C_5 and (C_6, two other terms derived from the Born approximation, are not fixed in the analytic fitting process, and therefore the only term fixed in the determination of constants in (1 ()) is C_7. This matter is discussed further in Sec. V. The constants for Eq. 10 derived in the iterative analytic fit are shown in Table I, along with the Born approximation constants. It is clear that the values of C_5 and C_6, obtained from the fit to the experimental data do not conform to the Born approximation values. There are, however, large uncertainties in these values, and in the following discussion we conclude that the uncoupled values of the 1st and 2nd order t('1'ills of the Born approximation may in any case diverge by large factors from the reality of the coupled system. The data and the analytic curve are plotted in Figure 9 with representative error bars indicating the calculated level of combined statistical and systematic uncertainty. Comparison of this result with previous measurements described

in the introduction is given in Table IV and Figure 10. The Long et al. data [1] is shown as renormalized by vanWyngaarden and Walters [8]. In addition, we have reanalysed the original Long et al. [1] data measured at 90° by correcting for polarization and cascade (in the manner described in Section III, III A and III E), renormalizing to the present cross section at 200eV.

1. Uncertainty in analytic quantities

Two factors contribute to the uncertainty in determining the experimental cross section, and in establishing the parameters in the modified Born approximation (Eq. 10). First, there is an unusual complexity in the shape of the cross section. The H (1s 2p) cross section shape appears to be unique among atomic cross sections in containing higher order terms significantly affecting the cross section into the high energy region. The evidence for this appears in both the experimental and theoretical CCC calculations. For this reason several parameters share in establishing the magnitude of the cross section into the high energy region, requiring an unusual range in energy to establish accurate parameter values. Defining the terms in Eq. 10 in the sequence $C_0 \ldots C_7$ as terms of order 7 0, we find that terms of order higher than 2 contribute about 50% of the total of 1('1 '111s above the zero order at 500 eV in both the CCC and experimental analysis. In contrast, at the same dimensionless energy (~ 50), a similar analysis (Ref. [46]) of the He ($^1S \quad 2^1P$) ("1'oss section indicates that terms of order higher than 2 contribute only about 1% of total ((.1'111S above zero order. For this reason the higher order terms in the case of He are intrinsically more accurately determined. It is only at values of dimensionless energy of ~ 2. that higher order terms significantly contribute for the He transition, a factor of 25 in dimensionless energy below the value at which similar effects occur for H. The second component contributing to uncertainty in the analysis is statistical and systematic errors in the measurements, generally less than 4%, as discussed in the Appendix.

The estimated 10% uncertainty in the present experimental result therefore stems primarily from the heavy mixing of the higher order terms in the analytic fit to the data. The uncertainty in the values of the first and second order terms in the analyzed experiment is large enough to encompass the values for these terms in the Born approximation, and therefore the terms are poorly constrained. The role played by the unique shape of the cross section is illustrated by the fit to the CCC calculations shown in Table 1. The analysis restricted to the energy range up to 1.8 keV shown in column 5 of the Table produces an error of 7% in returning the value of the zero order term, utilizing data considered to be internally accurate to 1 %. The difficulty in establishing accurate values of the higher order terms is discussed further in the examination the Ref. [20] CCC calculations

2. Conventional Normalization using a Bethe-Fano Plot

A conventional normalization procedure was also applied to the experimental data in the manner described in detail by Heddle and Gallagher [11]. In this approach, the experimental collision strength data is first corrected for polarization and cascade, and then placed on an absolute scale by fitting to the asymptotic Born limit at high energy defined by a Bethe Fano

line. The formulation for this line described by [11] is equivalent to relation 9a but without the C_6 term. The slope (determined from the constant C_7) is related to the known optical oscillator strength (8b) and the energy intercept is fixed using the Born value of C_5 (9b). On a plot of collision strength (cm^2 eV) vs Log(E(eV)), the resulting Bethe-Fano line has a slope of 6.129×10^{-15} cm^2 eV and an enegy intercept at 8.337 eV.

A fit of the experimental data to this Bethe-Fano line over the energy range 1-1.8 keV is shown in Figure 11. Values for the H (1s - 2p) cross section are listed in Table II). These data lie approximately 4.8% above the values obtained using the analytic fitting procedure and thus agree more closely with the CCC calculations of Bray [20]. The agreement is within 3% over the entire energy range of the experiment, as shown in Figure 12. At the critical energy of 54.4 eV, for example, the experimental H (1s - 2p) cross section derived using this approach is 0.713 au, compared to the CCC value of 0.729 au [20] and a value of 0.708 au quoted in the van Wyngaarden and Walters [8] analysis of the Long et al. data [1]. The better agreement of this result with the CCC calculations above 1 keV is due to the fact that the CCC calculations converge on the Born value for the 1st order (C_5) term. It is argued below that neither the experiment or the CCC calculations can define the value of C_5 to better than an order of magnitude, and that the probable value is roughly an order of magnitude smaller than Born.

B. Theoretical calculations

The literature is replete with calculated cross sections for the H (1s - 2p) transition. It is not the intent of this paper to review the merits of these published results. We refer the reader to the recent review by Ref. [4]. Considerations here are restricted to calculated cross sections in the work by Byron et al. [25], Bubelev et al. [17], and Bray [20]. The work by Ref. [25] is a unitarized eikonel Born series (UEBS) calculation that provides a useful comparison with the more recent [17,20] CCC and DWBA2 methodologies. The results of critical interest are the CCC calculations of Refs. [17,20], because it is argued that these values are at the ~1% level in internal accuracy. The analysis of the recent theoretical calculations [17,20] by fitting the results analytically using Eq. 10 indicate that the effects of multistate coupling extend significant influence on the cross section to energy in the range up to 1 keV. This introduces significant systematic uncertainty in the separation of the coefficients, as discussed above. The effect appears within the theoretical calculations, presenting uncertainty in determination of the values of the coefficients that should be used as an appropriate representation of the theory. For this reason we discuss the determination of the coefficients in more detail here.

1. Analysis of the CCC calculations

Table I (col 5) shows the coefficients derived in fitting Eq. 10 to the CCC calculations of Bray [20] to 1.8 keV, allowing all coefficients to be freely determined. As we have noted this results in a value of C_7, 7% larger than the Coulomb approximation (cf. Ref. [32]). The fact that the optical oscillator strength (which determines C_7 in Eq. 8b) is, however, a quantity internalized in the non-perterbative CCC calculation, the result represents uncertainty in the

fitting process caused by the heavy mixing of the terms in energy space. A more satisfactory result is obtained by fixing the value of the zero order constant to that given by Eq. 9(1. We find in analyzing the Ref. [20] calculations in this way, that the values of the higher 01"(1('1' terms vary systematically, depending on the value of the upper energy limit at which the data set is terminated. In principle, the values of the constants should be independent of the data termination point. In fact, the derived values of" the 1st and 2nd order constants in this case show a systematic downward trend in real numeric value, as a function of" decreasing truncation energy, as shown in Figure 13. The implication of the variation in Figure 13 is that the generalized oscillator strength implied from the CCC calculation is unstable in shape. Although determination of" uncertainty in the calculation is difficult, Bray [20] estimates that at intermediate energy ($\sim$ 50 eV) that the ('1'OSS section value is within 3% of reality ill the 90% confidence level, and at 1 keV, 5% at the 90% confidence level. The decreasing accuracy in the calculation toward higher energy is attributed to increasing amounts of cancellation in the numerical integration process (Ref. [20]). We use this estimate of accuracy in the calculation as a basis for choosing the energy range most shitable for deriving the Eq. I O 1(rm (oil Still nts. In this ('ii se we select the coefficients established in fitting the CCC data up to 200" eV as the most accurate representation of" the function. Table I (col 4) shows the derived constants for this (HISC, considered here to be the optimal fit to the CCC calculation. Figure 14 shows the percentage deviation of the fitted curve from the Bray [20] collision strengths. We note that the analytic function falls systematically below the CCC values at electron energies above 200 eV, deviating by about 3.6% at 1 keV. The analytic fit also falls below the Born approximation in the 1 keV region, conforming with the general tendency of Born cross sections to be larger than reality (Ref. [29,47], Figure 1). The analytic fit and the Ref. [20] collision strength values are compared in Figure 15.

2. Comparison of cross sections

The DWBA2 and CCC calculations converge 011 the Born approximation cross section near 1 keV. Although these calculations (lo not explicitly determine the terms in the Born equation, they tend to converge on the Born values at high energy (see Figure 1). The fact that the two higher 0] '(1('1' 1(erms in Eq. 9a depend on the shape of the generalized oscillator strength, indicates that the values of these terms in the Born approximation should deviate from reality in cases in which the cross section is significantly affected by interstate coupling. A computational method known as Born subtraction has been utilized in the theoretical calculations at high energy, which converges on the Born approximation (Ref. [17']). The CCC and DWBA2 calculations, however, (lo not accurately constrain the first and second order terms, because a 1 % error in the calculation at 1 keV translates into a large uncertainty in the higher order term values. The implication is that a systematic or statistical uncertainty in the calculated cross section at the level of 1% can produce an ('1'1'01" of order 10% in the oscillator strength derived r'1"0111 the data, caused primarily by the encroachment of multistate coupling effects into the 1 keV region.

The cross sections are compared numerically in Table III. It can be seen in Table 111 that the analytic fit to the experimental data falls below the Ref. [20] data by factors in the range 3 to 7% over the 2 keV energy band. The most remarkable aspect of the comparison of the CCC calculations of Ref. [20] and the analytic results derived from the current experimental

data is that the shape functions are very similar. The difference in shape is most easily observed in Figure 9, where the analytic fits to the CCC and experimental data are plotted in the form of collision strengths. The most significant difference appears in the 60 - 500 eV region (Figure 9) where the magnitude of the divergence is near the limit of experimental uncertainty. This region in electron energy is, however, the most vulnerable region for errors to occur in the present experiment.

Table III includes the DWBA2 calculations of Ref. [17] and UEBS results from Ref. [25]. The Ref. [17] DWBA2 cross sections are significantly larger than the CCC, UEBS, and the present experimental results at and below 150 eV (see Figure 1). The CCC calculations reported by [17] (not shown here) are insignificantly different from the Ref. [20] values. The analysis of the present experimental results are within 3% of the UEBS Ref. [25] calculations (Table III).

V. DISCUSSION AND CONCLUSIONS

The most important consideration in the comparison of the experimental data with the theoretical results is the shape of the cross section. We find, as shown in Sec. IV that the shape of the analyzed experimental data conforms to the recent theoretical CCC calculations (Refs. [17,20], see Figure 9) within estimated uncertainty. The analysis of both the experimental and theoretical CCC results using a modified Born approximation, described in Sec. IV, indicates that higher order terms influence the cross section to an unusually high energy. The effect of this is to increase the uncertainty in the experimental absolute cross section derived from the analytic fit, to an estimated 10%, while statistical and systematic uncertainties were limited to 2%. A similar analysis of the Ref. [20] CCC calculations setting an upper bound in energy at the same level as the experimental data, produced a similar error (in the opposite direction) in the value of the derived optical oscillator strength (Table 1). This is a clear indication that the accuracy of this or any other methodology is limited in this particular case primarily by the subtle changes in shape function reaching into the high energy region. The unique nature of the shape is presumed to be caused primarily by the strong coupling of the 2s and 2p states (Ref. [20]). The difficulty in separating the higher order terms is illustrated in the analysis of the CCC calculations shown in Figure 13. This Figure shows the variation in the 1st and 2nd order terms in the analysis of the Ref. [20] CCC data as a function of the energy of the upper truncation point in the analyzed data set. One can see from the Figure that the C_5 and C_6 values are ("10s(" to the values of the Born approximation constants (Table I) for truncation energies at or above 1keV. At 500" eV (Figure 13), however, the values of the constants suddenly drop in the optimal fitting process by factors of about 2 and 4. The uncertainty in the constants derived from the experimental data is at least this large. At lower energies the real numeric values of the constants continue to decline systematically in the analysis of the CCC calculations, as shown in Figure 13. 111 principle the constants should be invariant in Figure 13. Although the form of the analytic formulation may play a small role in defining this variation]), very small computation errors within the stated uncertainty (Ref. [20]) can easily be responsible for the behavior shown in Figure 13. The accuracy of the analytic fit to the CCC data is shown for the selected case in Figure 14 where the maximum deviation in the fit is 3.3% at 1 keV, and generally in the range less than 0.5% at energies below 500 eV. We select

the constants in the analytic terms for the fit to the CCC calculations by Bray [20] for the 200 eV case as the recommended representation of the CCC cross section (Table 1, col. 4). This produces cross sections that fall below the Born approximation at energies in the 1 keV range, by about 3%, consistent with the argument that the higher order constants in the Born approximation are upper limits to the coupled system constants (Ref. [29,47]; see Figure 1). The collision strengths derived from CCC (Ref. [20]) and experimental results are compared in Figure 9. The numeric values of the cross sections are compared in Table III.

We summarize our conclusions with the following points.

1. We conclude on the consideration of the combined effects, that the accuracy of the absolute cross section derived from the experimental measurements reported here for the 11 (1s 2p) transition are limited to about 10%.

2. The strong coupling evident in the analysis of both the theoretical and experimental results suggests that the shape of the generalized oscillator strength deviates significantly from the Born 1S 2p shape function (Eq. 7). The 1st and 2nd order terms in the modified Born approximation are therefore expected to deviate substantially from the uncoupled values. The experimental and theoretical CCC results, however, do not put strong constraints on the values for the coefficients of these terms, implying uncertainty in the exact shape of the generalized oscillator strength. The 1st order constant derived from the experiment and analysis of the CCC calculations are substantially smaller than the uncoupled Born value. The experimental cross section and analysis of the CCC calculations depend on knowledge of the optical oscillator strength for the H (1s ?))) transition. It has been assumed that the value of this constant is unaffected by coupling effects. This is a reasonable expectation given that the major coupling effect is 2s 2p.

3. We recommend, on the ground that (within stated error bars) the experiment is consistent with the Ref. [20] CCC calculations, that the analytic coefficients derived from the CCC results given in Table 1, col. 4, be utilized as a cross section model for electron impact energies from 15 eV to 5 keV. For astrophysical purposes, there is no practical difference between the present experiment and the Ref. [20] results. Table V lists values of the recommended cross section for selected energies. Resonance and exchange effects, not determined here, must be included to define the cross section to 1111'(s1101(1. The near threshold H (1S 2p) cross section and a model of the general discrete atomic hydrogen emission properties (11 (n(n()) will be given in a following paper (Ref. [31]).

ACKNOWLEDGMENTS

This work was carried out at the Jet Propulsion Laboratory, California Institute of Technology, and the University of Southern California. The work at the Jet Propulsion Laboratory was supported by the Atomic, Molecular and Optical Physics program of the National Science Foundation (Grant # PHY- 9220742), the Astrophysics and Planetary Atmospheres programs of the National Aeronautics and Space Administration, and by the

Air Force Office of Scientific Research. The work at the University of Southern California was supported by the National Science Foundation (ATM-9320589) and NASA (Grant NAGW-3905). J. W. McConkey acknowledges support from the Natural Sciences and Engineering Research Council of Canada. The authors are particularly grateful to Igor Bray for generously providing us with the unpublished results of his latest CCC calculations for Q_{1s2p}, Q_{1s3s}, and Q_{1s3d}. In addition, we gratefully acknowledge Don Madison and Vladimir Bubelev for providing us with their DWBA2 calculations, and James Walters for supplying us with the results of his First Born calculation. We have benefited greatly from discussions with all of the above. The authors also wish to acknowledge Bill Lanigan for his invaluable assistance in the design and implementation of the computer control of the experimental apparatus.

APPENDIX: ANALYSIS OF ERRORS INTERNAL TO THE EXPERIMENT

A comprehensive analysis of statistical and known systematic errors was performed in order to determine the limiting accuracy of the present measurements. The additional factors involved in establishing absolutes values from the analytic fit to the data are discussed in Section IV. Sources of error in the measured signal are detailed below.

1. *Variations in electron beam current and hydrogen source pressure:* The experimental system is interfaced to a PC-based data acquisition and control system which monitors critical parameters of our experiment and normalizes the measured signals to the electron beam current and hydrogen source pressure, eliminating known sources of systematic error. Data are accumulated in a multiple scanning mode to reduce the effects of drift in other experimental parameters.

2. *The measured dissociation fraction:* Since the dissociation fraction (1)) is needed for subtraction of the molecular Lyman-α contribution to the observed signal, the uncertainty in the derived atomic signal produced by the error in the measured value of D. Measurement of the dissociation fraction has a relative of $\sim \pm 3\%$, based on the signal statistics of the discharge on and off measurements performed at the I.() III II. For a (typical) dissociation fraction of 0.65, this and in the molecular subtraction procedure of $\pm 0.2\%$ for the electrostatic gun data, and of $\sim \pm 1\%$ for the magnetic gun data, reflecting the lower signal rates of the latter. The accuracy of the subtraction is demonstrated in Figure 6.

3. *Statistical errors in the observed signal count rates:* The statistical error (assuming a Poisson distribution) in the net signal varies since the signal flux changes with energy and is also different for the electrostatic and magnetic gun configurations. For the electrostatic gun, the signal statistics varied from $\pm 0.3\%$ at 200 eV to $\pm 0.6\%$ at 1.8 keV. For the magnetic gun data, the statistical varied from $\pm 3.2\%$ near threshold to $\pm 2.6\%$ at 200 eV.

4. *Error in the polarization correction.* Since the signal flux obtained at 90° must be corrected by the factor $(1P/3)$ in order to derive the total cross section, an error is

introduced from the uncertainty in the polarization. Polarization data for H Lyman-α measured by Ott et al. [9] have reported absolute error bars of ± 0.01 or less in the region from threshold to 200 eV. This results in a relative error of up to $\pm 0.3\%$ in the polarization correction procedure. For energies above 200 eV, the McFarlane formulation [38] (equation 11) for the polarization was used. Although a realistic estimate of the error in the McFarlane approach is not possible, the polarization fractions are, in any case, relatively small in this energy region (maximum ~ 0.1), and the resulting error can be safely taken to be negligibly small.

5 *Detector background subtraction:* The detector background subtraction is particularly important at the highest electron impact energies where the signal strength is lowest and the accuracy of the normalization procedure is critically dependent on the quality of the experimental data. This background was measured to an accuracy of $\pm 2\%$, which results in an error of up to $\sim \pm 0.2\%$ in the determination of the atomic signal at the highest energy.

6 *Quenching of H(2s):* Deactivation of 2s metastable atoms into the 2p state within the field of view of the detector would introduce an erroneous component to the signal. The interaction region was, however, rigorously shielded to ensure the absence of stray fields. In the case of possible fringing fields from the biasing voltages applied to the Faraday Cup, a systematic investigation of the Lyman-α signal, as a function of these voltages, revealed no statistically significant dependence on stray fields from this source. We conclude that there is no significant contribution to the signal arising from quenching of the 2s metastable population by field effects. The electron beam in addition to exciting the 2s state, also deactivates into the 2p state with a collision strength of about 600 au (see [48]). The maximum beam current in this experiment is 18 μA at 12 eV, corresponding to a deactivation time of about 2 msec. Electron collisions therefore dominate the deactivation process. The effect, however, is negligible in this case because of the very short lifetime of the H atoms in the beam compared to the production and deactivation lifetimes. The steady state 1110(1 ('1 calculations determining the cascade contribution were for this reason carried out neglecting the 2s 2p collisional transition (see [31]).

7 *Errors associated with magnetic field confinement of the electron beam:* The use of magnetic confinement to produce the electron beam can lead to errors arising from energy dependent path length differences in the interaction region due to the helical trajectories of the electrons. At very high electron densities there is also the possibility of non-linearities in the beam profile due to space charge induced scalloping of the beam. Using the correction factors described by Taylor et al. [49] we estimate that path length variations of our electron beam are negligible at energies up to 200eV used in the present experiment. In the case of scalloping, we were (ill" (f(l touse electron currents well below the space charge limit at each energy. We believe that any effects associated with magnetic field confinement are not significant in the present experiment. Indeed, the similarity between the shapes of the renormalized excitation function data of Long et al. [1] shown in Figure 10 and the present work adds additional confidence to this claim since the Long et al. [1] data from threshold to 200 eV were

obtained with an electrostatic gun in the absence of any magnetic field. The use by Ref. [1] of an electrostatic gun at low electron impact energies was possible since the atomic H target was a swarm not a beam, eliminating systematic effects due to variation in electron beam profile with energy

8. *Errors associated with low energy secondary electrons:* Historically, excitation function measurements have been plagued by problems associated with the presence of secondary electrons in the interaction region. These electrons can cause further excitation, leading to erroneous signals, especially in the critical high energy region where data are normalized and where a relatively small secondary component can lead to a disproportionately large contribution to the atomic signal. Secondary electrons are a particular problem for magnetic guns, where electrons produced in ionizing collisions and at gun apertures, can be trapped in the confining magnetic field. The selection of an electrostatic gun for the energy region above 200 eV ensures the absence of any magnetically trapped secondary electrons. It should also be noted that we could not get acceptable fits to our data at high energies to the Born limit using our magnetic gun.

9. *Error in the cascade correction:* This is a difficult error to quantify since our cascade corrections depend on the accuracy of various theoretical calculations, as described in Section 3.5. The magnitude of the cascade correction is highly dependent on energy, decreasing from a ~27% correction near threshold to ~3% at 1.8keV. It has been pointed out by van Zyl and Gealy (1987) that small electric fields can significantly perturb the cascade contribution. Errors in cascade corrections can be a significant factor in the accuracy of our Q_{1s2p} data, especially at energies below 40 eV, where the corrections are large. In presenting our data, we have assumed an uncertainty of ±10% in the cascade corrections at all energies.

The above errors are combined appropriately in quadrature to obtain values for the total experimental error in (a) the measured Lyman-α signal and (b) the derived relative Q_{1s2p} values. For the electrostatic gun data, the resulting calculated error in (a) increases from ±0.3% at 200 eV to ±1.8% at 1.8 keV. The corresponding errors in (b) are ±0.5% and ±1.9%, respectively. For the magnetic gun data, the error in (a) is ~±3.4% near threshold, reducing to ±2.8% at 200 eV. The corresponding errors in (b) are ~±4% near threshold, reducing to ~± 2.9% at 200 eV.

The analytic fitting of the experimental data using Eq 10 reduces the statistical contribution to the uncertainty in data values to a negligible contribution relative to the systematic errors. The effect of the systematic factors is discussed in Sec. IV

REFERENCES

[1] R. 1,.1,0,, g, D. M. Cox and S. J. Smith, J. Res. Nat. Bu r. Sta nd. Sect. A: Phys. Chem. **72A,** 521 (1968).

[2] J. F. Williams, J. Phys. B: A t. Mol. Phys. **9**, 1519 (1976).

[3] J. F. Williams > J. 1'11}'s. B: At. Mol. 1'11)'s. **14,** 1197 (19s1).

[4] S . Trajmar and 1 in *Atomic and Molecular Processes in Fusion Edge Plasmas* . edited by R. K. Janev (Plenum, New York, 199[]), p.31.

[5] G. C. King, S. Trajmar and J. W. McConkey, Comm. Atom. Mol. Phys. **23**, 229 (1989).

[6] W. L. Fite and R. T. Brackmann, Phys. Rev. 112, 1 151 (1958).

[7] J. W. McGowan, . 1 . F. Williams and E. K. Curl ey, Phys Rev. **180**, 132 (1969).

[8] W. L. van Wyngaarden and H. R. J. Walters, J. Phys. B: At. Mol. Phys. **19**, L53 (1986).

[9] W. R. Ott, W . E. Kauppila and W. L. Fite, 1'11)'s. Rev. A 1, 1089 (1970).

[IO] D. J. '1'. Morrison, and **M.** R. H. Rudge, **(1966)** 1)1"()(". Phys. Soc. **89** , 45 (1966).

[11] D. W. O. Heddle and J. \ \ '. Gallagher, Rev. Mod. 1'11)"s. **61,** 221 (1989).

[12] 1,. A. Vainshtein, Opt. Spectrosc. **18.** 538 **(** 1 965).

[13] U. Fano, Phys. Rev. **95**, 1 198 (1954)

[14] D. H. Madison, Comm. Ate])]. Mol. Phys. **26**, 59 (1991).

[15] P. J. M. van der Burgt, W. B. Westerveld and J. S . Risley, J. Phys. Chem. Ref. Data 18, I 757 (1 989).

[16] 1). E. Shemansky, J. M. Ajello and 1). 'P. Hall, Ap. J. **296**, 765 (1985).

[17] V. E. Bubelev, D. H. Madison, 1. Bray and A. T. Stelbovics, J. Phys B: At. Mol. Opt. Phys. 28, 4619 (1995).

[18] P. G. Burke, 1{. A. Berringtonand (~. \'. Sukumar, J. Phys. B. At. Mol. Phys. **14**, 289 (1981).

[19] 1. Bray and A. 'P. Stelbovics, Phys. Rev. A **46**, 6995 (1992).

[20] I. Bray, (private communication) (1996).

[21] J. Callaway and K. Unnikrishnan, Phys. Rev. A **48**, 4292 (1993).

[2'2] W. L. van Wyngaarden and H. R. J. Walters, .1. Phys. B: AI. Mol. Phys. **19**, 929 (1986).

[23] M. 1). Scott, **'1'.** T. Scholz, 11. R. J. Walters and 1'. G. Burke, J. Phys. B: Al. Mol. Opt. Phys. 22, 3055 (19s9).

[24] A . E. Kingston and H. R. J. Walters, J. Phys. B. Atom. Molec. Phys., **13**, 4643 (1980).

[25] F. W. Byron Jr., C. J. Joachain, and R. M. Potvliege, J. Phys. B: A t. Mol. Phys **18** , 1637 (J 985).

[26] A. R. Filipelli, C. C. Lin, 1,. W. Anderson and J. W. McConkey, (1991), Adv. Atomic Mol. Phys. **33**, 1 (1994).

[27] N . F. Mott and H. S. W. Massey, in *The The ory of A tomic Collisions*, t hird edition (Clarendon, Ox ford, 1 965) p.475.

[2S] M. Inokuti, Rev. Mod. Phys. **43** , 297 (1971).

[29] 1). R. Bates, A. Fundaminsky, and H. S. W. Massey; Part I, D. R. Bat es, A. Fun - daminsky, J. W. Leech, and **11. S.** W. Massey; Part 11, Phil. Trans. Roy. Soc., **A 243**, 93 (19[]0).

[30] 1). E. Shemansky, J. M. Ajello, D. 'P. Hall and B. (). Franklin, Ap. J. **296**, 774 (1985).

[31] 1). E. Shemansky, G. K . James and J. A. Slevin, Ap. J. (to be published)

[32] D. R. Bates, and A. Damgaard, Phil. Trans. Roy. Soc ., **A 242**, 101 (1949).

" Kimball Physics, Inc., 311, Kimball Hill Road, Wilton, NH 03086 9742.

[33] J. M. Ajello, D. E. Shemansky, B. O. Franklin, J Watkins, S. Srivastava, G. K. James, W. T. Simms, C. W. Hord, W. Pryor, W. McClintock, V. Argabright and D. Hall, Appl. Opt. **27**, 890 (1988).

[34] G. K. James, J. M. Ajello, I. Kanik, B. C. Franklin and D E. Shemansky, J. Phys At. Mol. Opt. Phys. **25**, 1481 (1992).

[1] Lab Windows, National Semiconductor.

[35] J. A. Slevin and W. Stirling, Rev. Sci. Instrum. **52**, 1780 (1981).

[36] P. N. Clout and D. W. O. Heddle (1969), J. Opt. Soc. Am. **59**, 715 (1969).

[37] F. G. Donaldson, M. A. Hender and J. W. McConkey, J. Phys. B: At. Mol. Phys. **5**, 1192 (1972).

[38] S. C. McFarlane, J. Phys. B: At. Mol. Phys. **7**, 1756 (1974).

[39] I. C. Percival and M. J. Seaton, Philos. Trans. R. Soc. London, Ser A **251**, 113 (1958).

[40] J. L. Forand, S. Wang, J. M. Woolsey and J. W. McConkey, Can. J. Phys. **66**, 349 (1988).

[41] J. M. Woolsey, J L. Forand and J. W. McConkey, J. Phys. B: At. Mol. Phys. **9**, 493 (1986).

[42] D. E. Shemansky, G. R. Smith, J. Geophys. Res., **86**, 9179 (1981)

[43] B. Van Zyl and M. W. Gealy, Phys. Rev. A **35**, 3741 (1987).

[44] B. Van Zyl, B. K. Van Zyl and W. B. Westerveld, Phys. Rev. A **37**, 4201 (1988)

[45] W. J. Karzas and R. Latter, Ap. J. Suppl. **6** , 167 (1961).

[46] D. E. Shemansky, J. M. Ajello and D. T. Hall, Ap. J. **296**, 765 (1985).

[47] D. W. O. Heddle, Adv. Atom. Mol. Phys. 15, 381, Academic Press, New York (1979). Nat. Bur. Stand., NSRDS NBS 25, Aug. (1968).

[48] E. M. Purcell, Ap. J., **116**, 457, (1952).

[49] P. O. Taylor, K. T. Dolder, W. E. Kauppila and G. H. Dunn, Rev. Sci. Instrum, **45**, 538 (1974).

[50] K. H. Schartner, private communication, 1995.

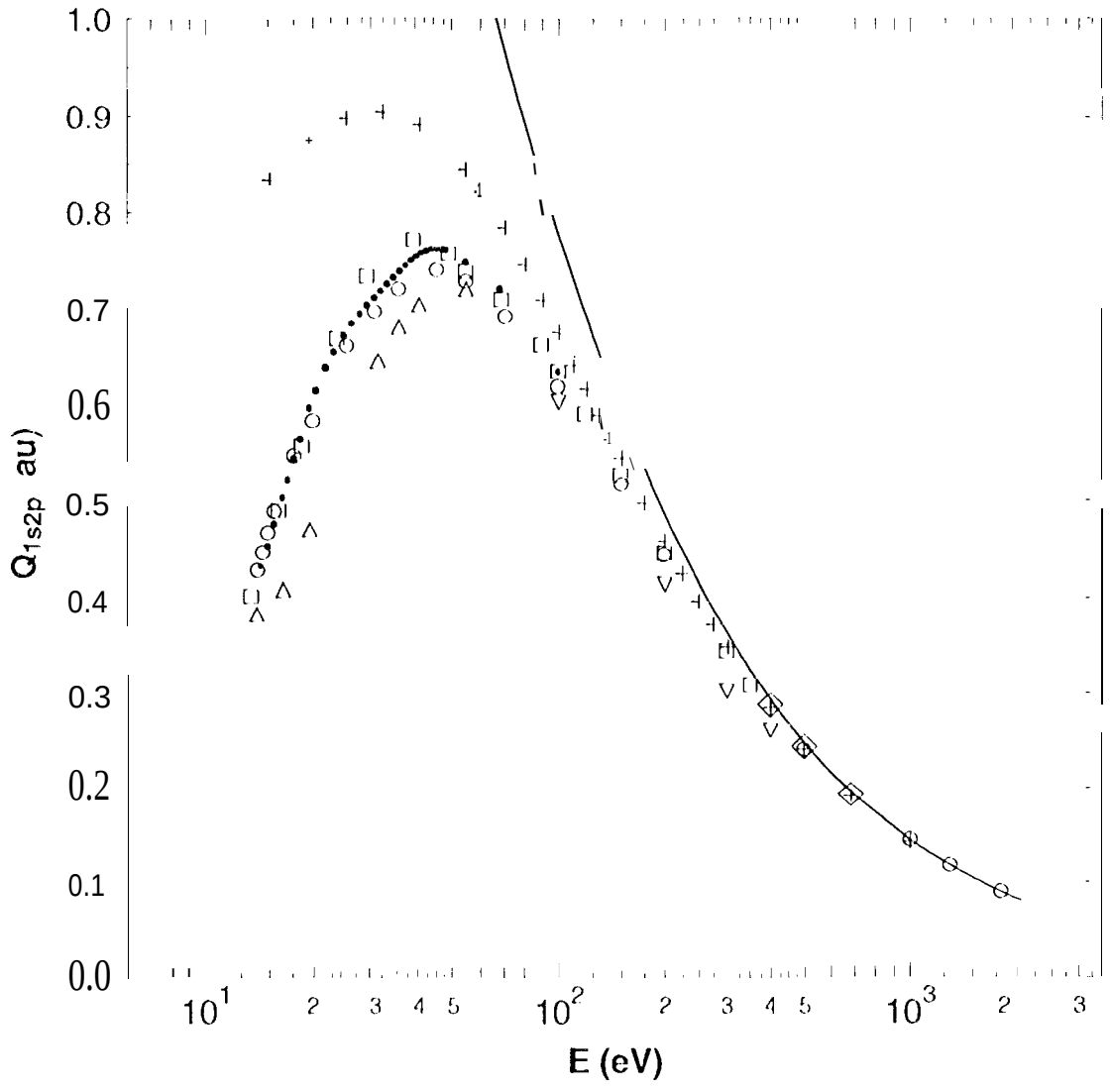

FIG. 1. Summary plot of theoretical H (1s - 2p) cross sections. The calculation methods can be categorized into various approaches: Born approximation (solid curve); Coil\'clp, ('llt close coupling (CCC) calculations of Bray [20] (open circles); multi-pseudo state calculations of van Wyngaarden and Walters [8], [2?] (open squaws), Scott et al. [23] (up triangles), Callaway and Unnikrishnan [21] (dots) ; second order distorted wave Born approximation (DWBA2) calculations of Kingston and Walte rs [24] (open diamonds), Bubelev et al. [17] (pluses); unitarized eikonal Bor n series (UEBS) calculations of Byron et al. [25] (down triangles).

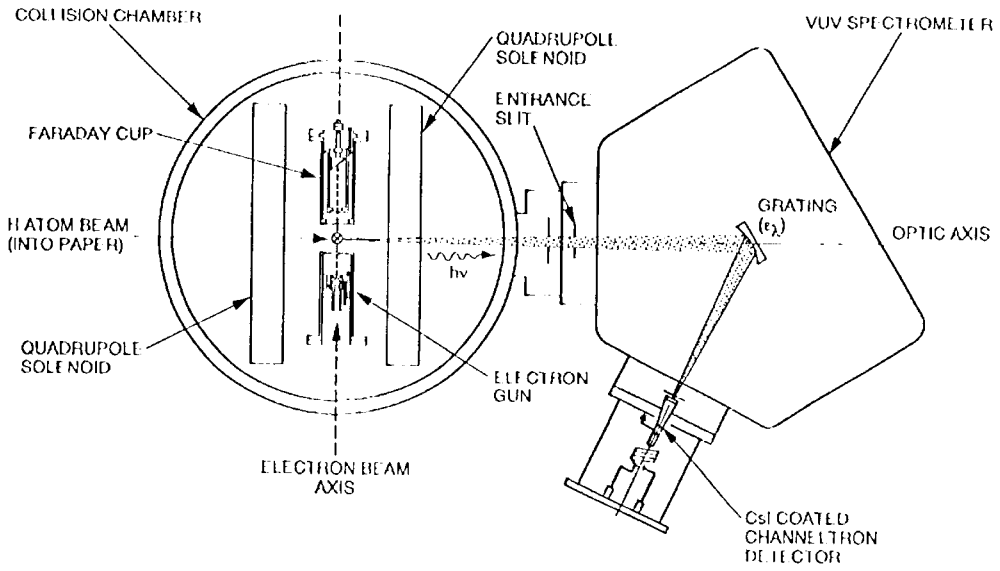

FIG. 2. Schematic top view of the experimental apparatus showing the electron impact collision chamber in tandem with a 0.2 meter VUV monochromator and CsI-coated channeltron detector. A 3 element electron gun is shown in which the beam is confined by the axial magnetic field produced by 4 solenoids arranged in a quadrupole configuration. This magnetic gun is used for measurements from threshold to 200 eV. The atomic H beam is produced by the RF discharge source shown in Figure 4.

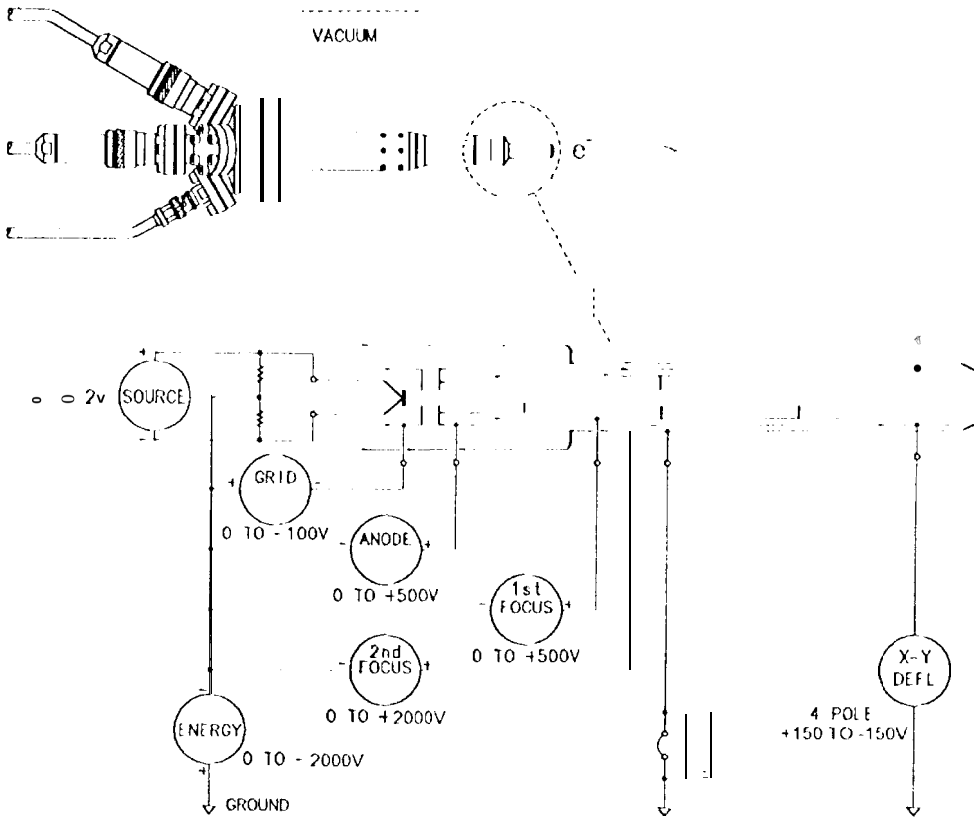

FIG. 3. Schematic diagram of the electrostatic electron gun and associated electronics. A unipotential refractory metal cathode produces an electron beam of low energy spread ($\sim$0.3 eV). The lens design enables a constant focal plane position and spot size to be maintained over the energy range in which measurements are made (200 1.8 keV). Typical beam currents are $\sim$5 μA. The X and Y deflectors provide beam steering capability.

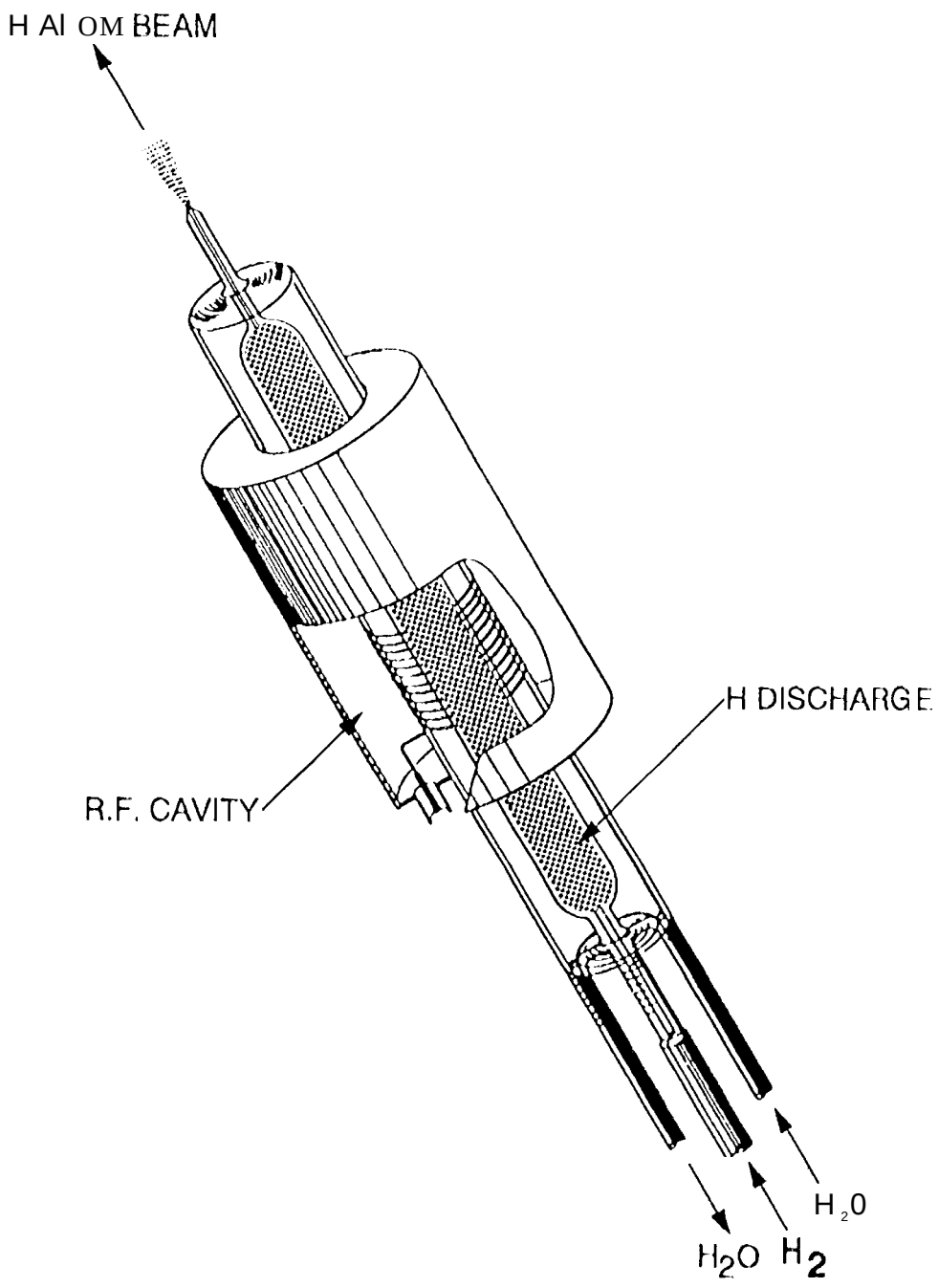

FIG. 4. Schematic diagram of the RF discharge source (Ref. [35]). Molecular hydrogen (purified by passing through a palladium finger) is dissociated in a discharge excited within an RF cavity, resonant at 36 MHz. The pyrex discharge tube is water cooled. A typical dissociation fraction, measured at the interaction region, is 0.65 ± 0.02.

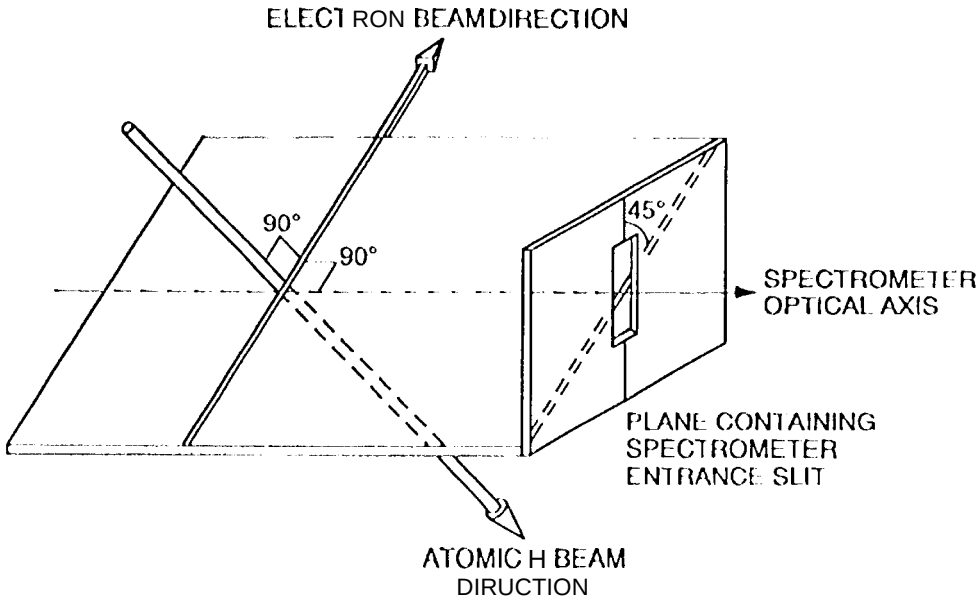

FIG. 5. Orientation of the electron and atom beams with respect to the monochromator (Ref. [34]). By rotating the monochromator such that the plane defined by the entrance slit and optic axis is at 45° to the electron beam axis, effects due to the polarization sensitivity of the detection system are eliminated.

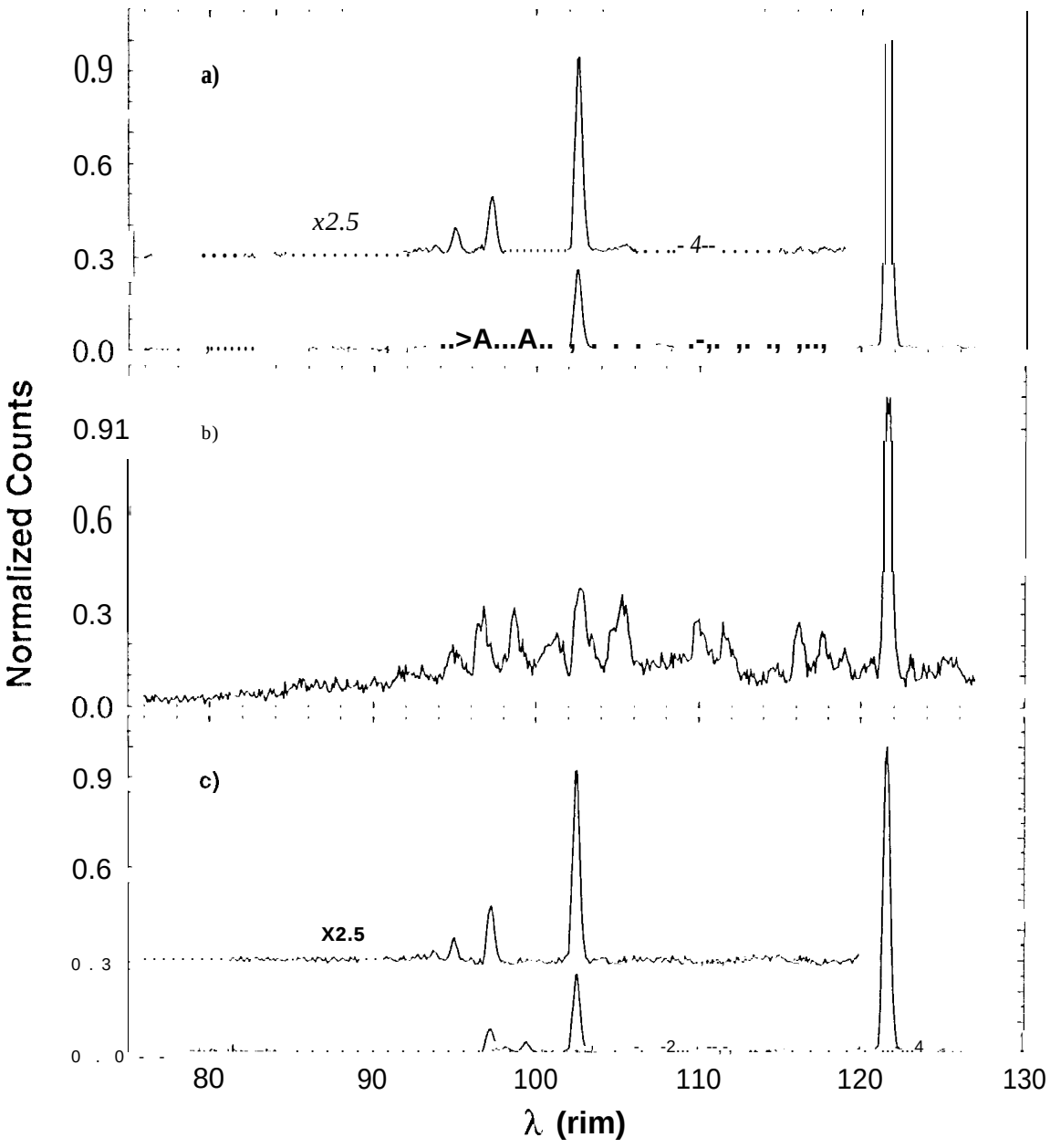

FIG. 6. Emission spectra produced by electron impact excitation at 100eV of a partially dissociated target beam (discharge 011) and an undissociated molecular target beam (discharge oil') are shown in a) and b), respectively, at a resolution of 0.5nm (FWHM). Application of the molecular subtraction procedure described in Sec. III yields the net (e+H) spectrum shown in c) in which Lyman series members up to n = 6 can be identified.

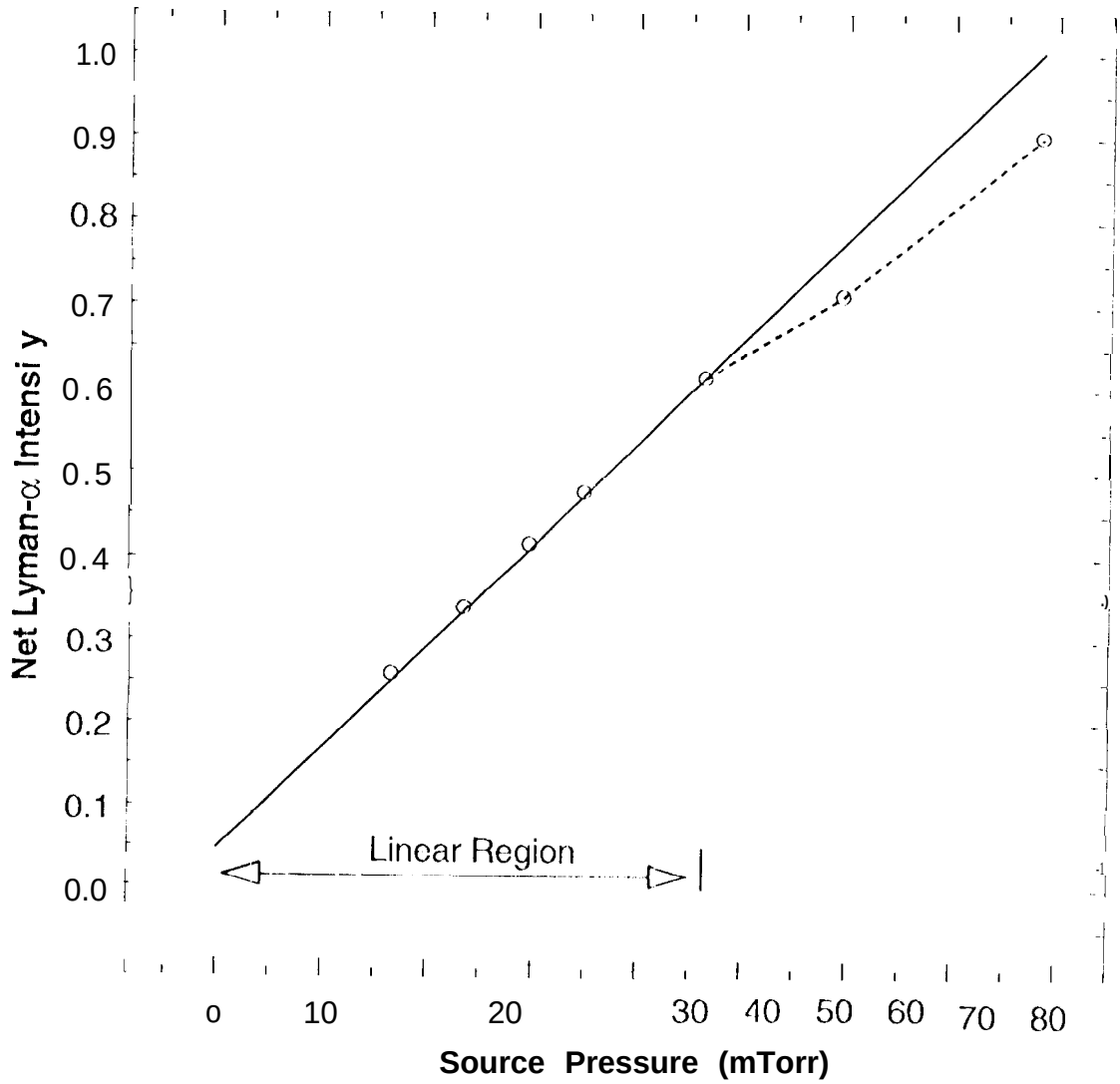

FIG. 7. Plot showing the net (e+H) Lyman-α intensity measured at 100 eV as a function of discharge source pressure. The dissociation fraction is measured at each pressure together with the signals obtained with the discharge on and off. Net (e+H) Lyman-α intensities are obtained using the procedure described in Sec. III. Operation of the source at pressures less than ~46 mTorr ensures the absence of resonance trapping effects.

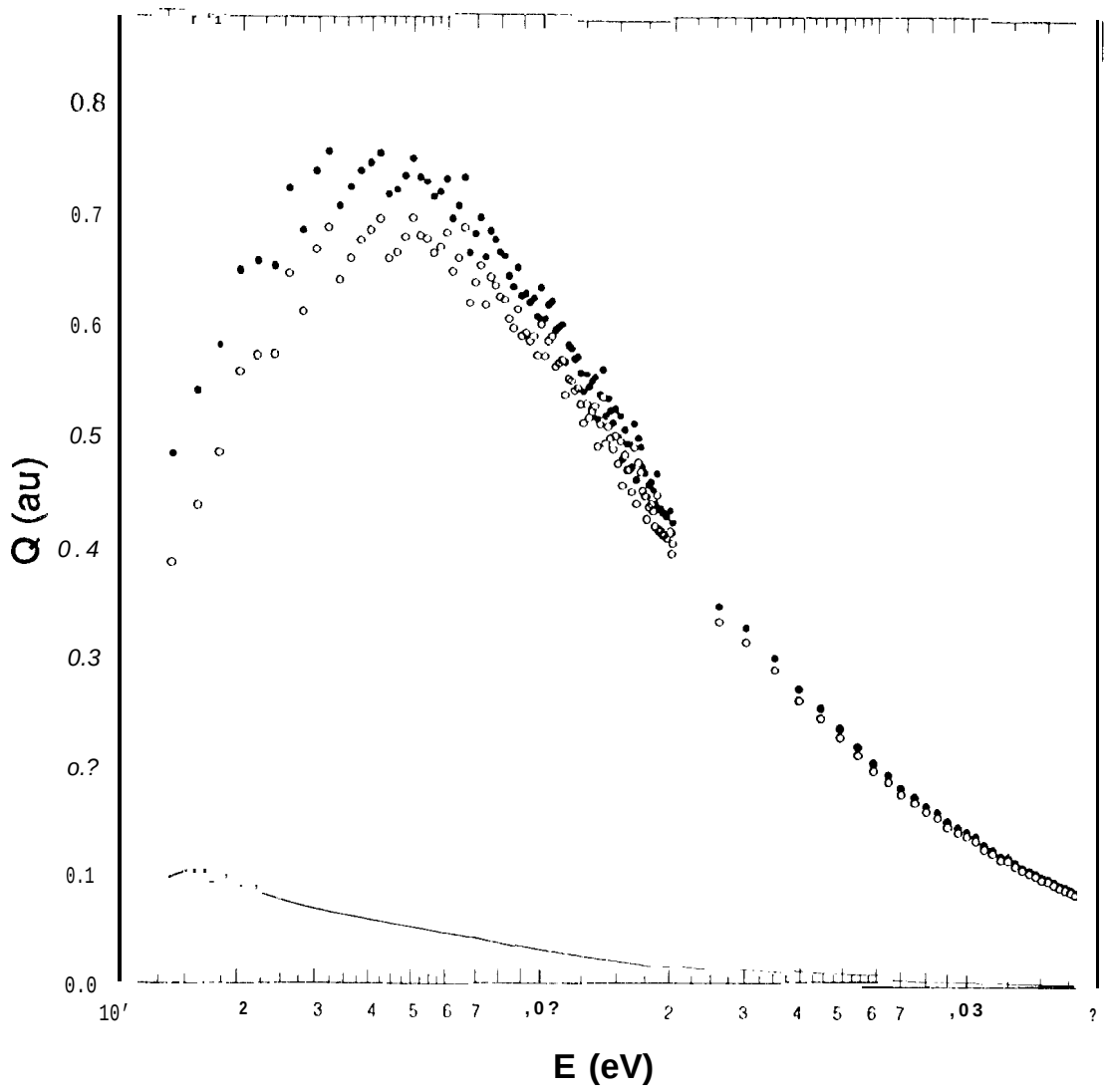

FIC. 8. The effect of cascade on the measured 11(2[)) ("1'oss section. The calculated (1(Cf. [31]) cascade cross section for populating the 11 (2p) state by electron excitation, shown as a solid line, compared to the experimental **II** (1s 2p) emission cross section, shown as solid circles. The experimental data has been corrected for polarization effects. The open circles are the experimental data after subtraction of the calculated cascade.

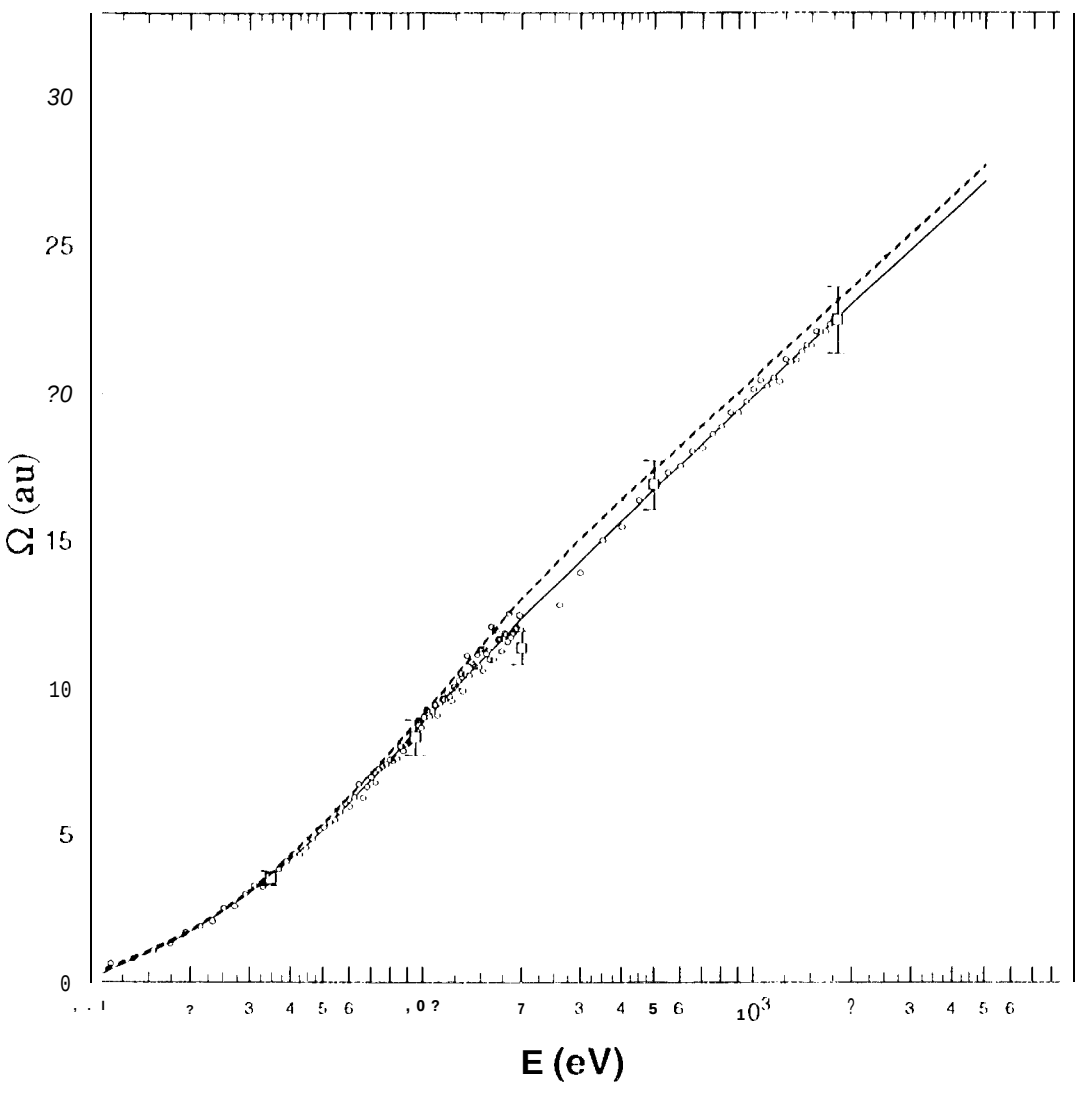

FIG. 9. Experimentally derived collision strength for electron excitation of the H (1s–2p) transition (open circles), compared to an analytic fit to the data using Eq. (10) (solid line), and similar analytic fit to the Bray [20] CCC calculations truncated at 200 eV (dashed line). Representative error bars shown on the figure are estimated combined statistical and systematic uncertainty. Coefficients for the analytic curve are given in Table 1.

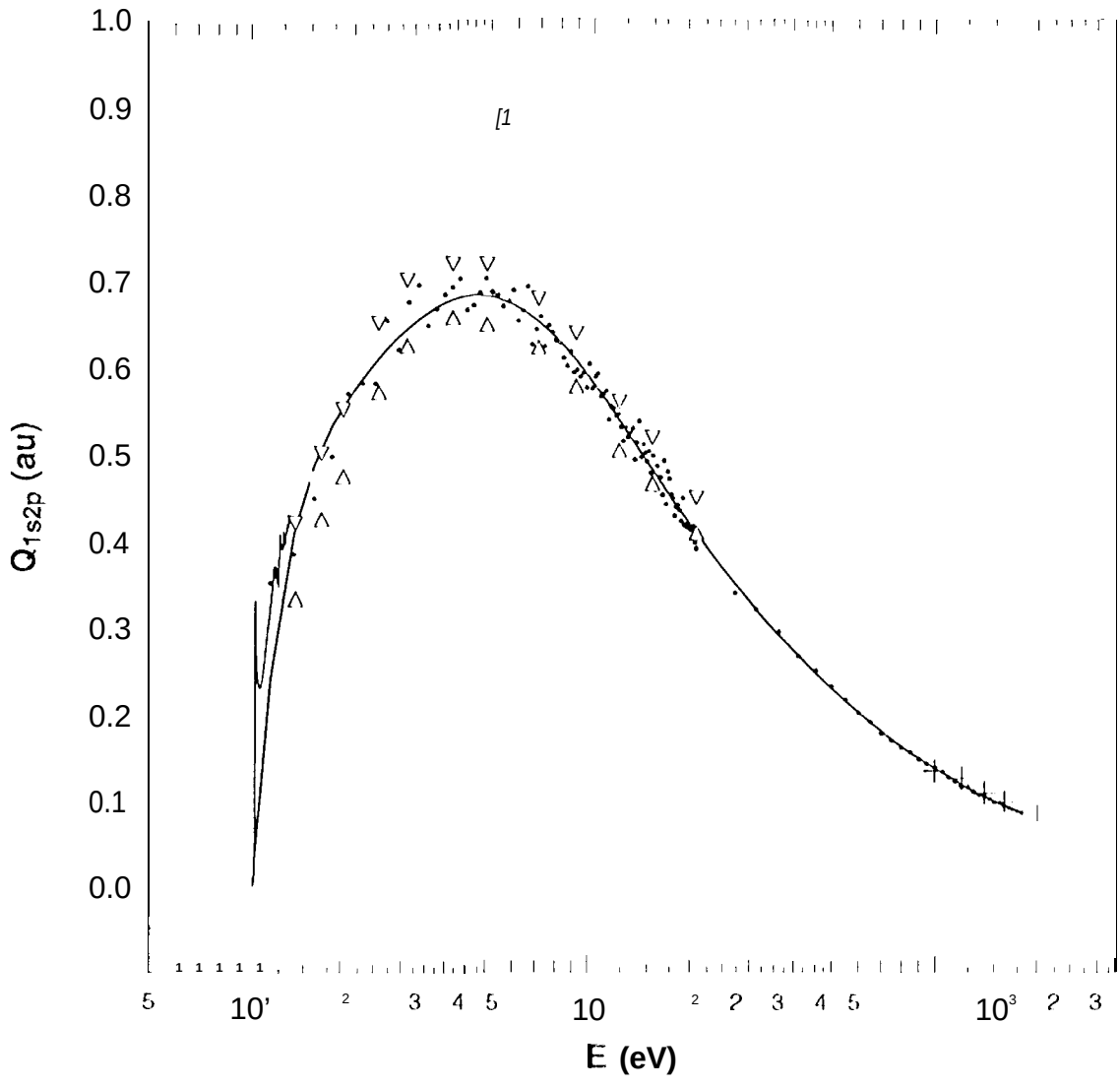

FIC . lo. Summary plot of experimental 11 (IS 2p) cross sections. Dots: p resent work; thick line: analytic fit to present data set; thin line: William s [2] threshold data; open square: Williams [3]; up triangle: Long et al. [1] data corrected for polarization (u sing Ref. [9]) and cascade (usi ng present model [31]) then normalized to p resent cross section at "200" eV; down triangle: Long et al. [1] data corrected by van Wyngaarden and Walters [8] for polarization and cascade and nor malized to their theoretical value at 200 eV; pluses: Schartner [50].

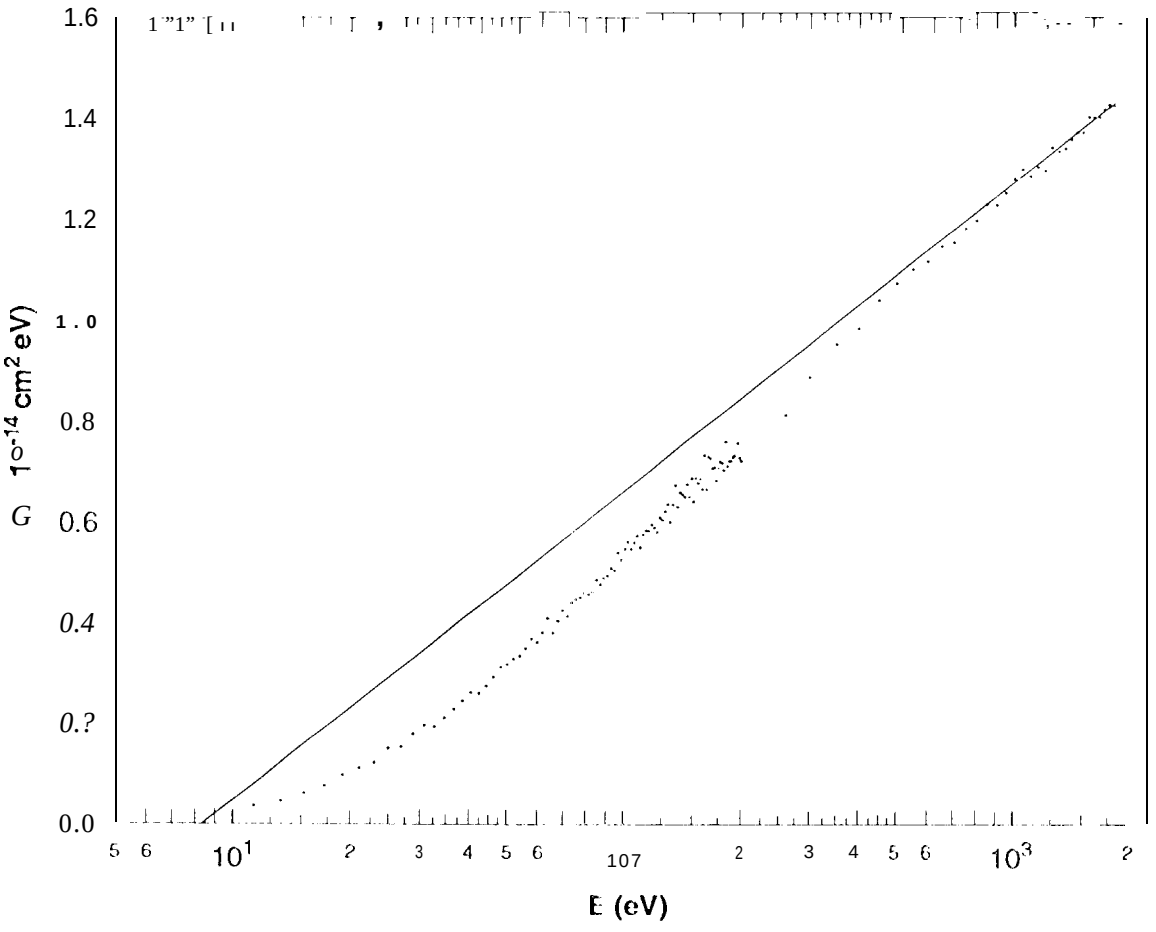

FIG. 11. Experimental H(1s 2p) collision strength data ((1ots) normalized by fitting to a Bethe Fano line (solid) in the high energy region from 1 keV to 1.8 keV in the manner described by Heddle and Gallagher [1 1]. The slope and intercept of the Bethe-Fano line are defined by Born constants.

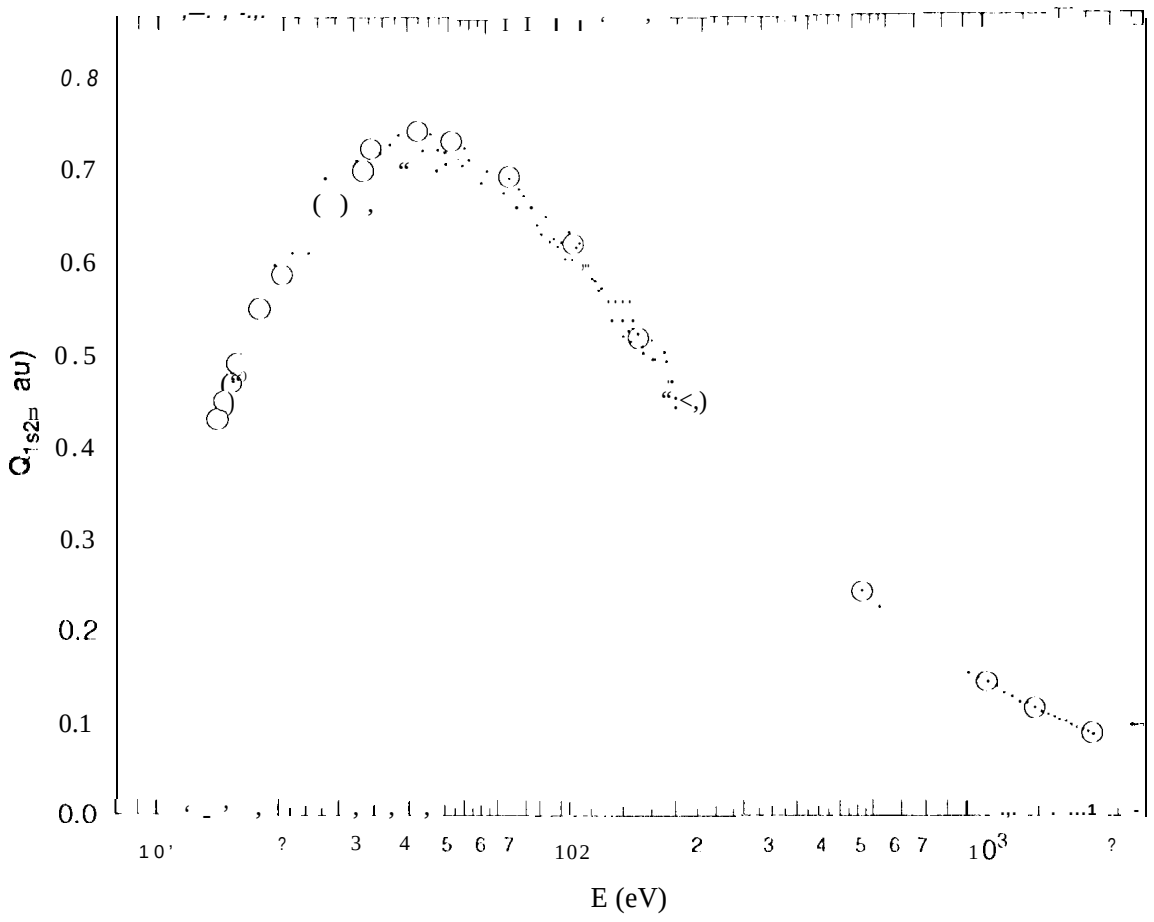

FIG. 12. Experimental H(1s - 2p) cross section (dots) derived from a conventional Bethe Fano normalization procedure compared to the theoretical CCC calculations of Bray [20] (open circles). The experimental cross section values and the Bray[20] values above 500 eV are an upper limit to the true cross section.

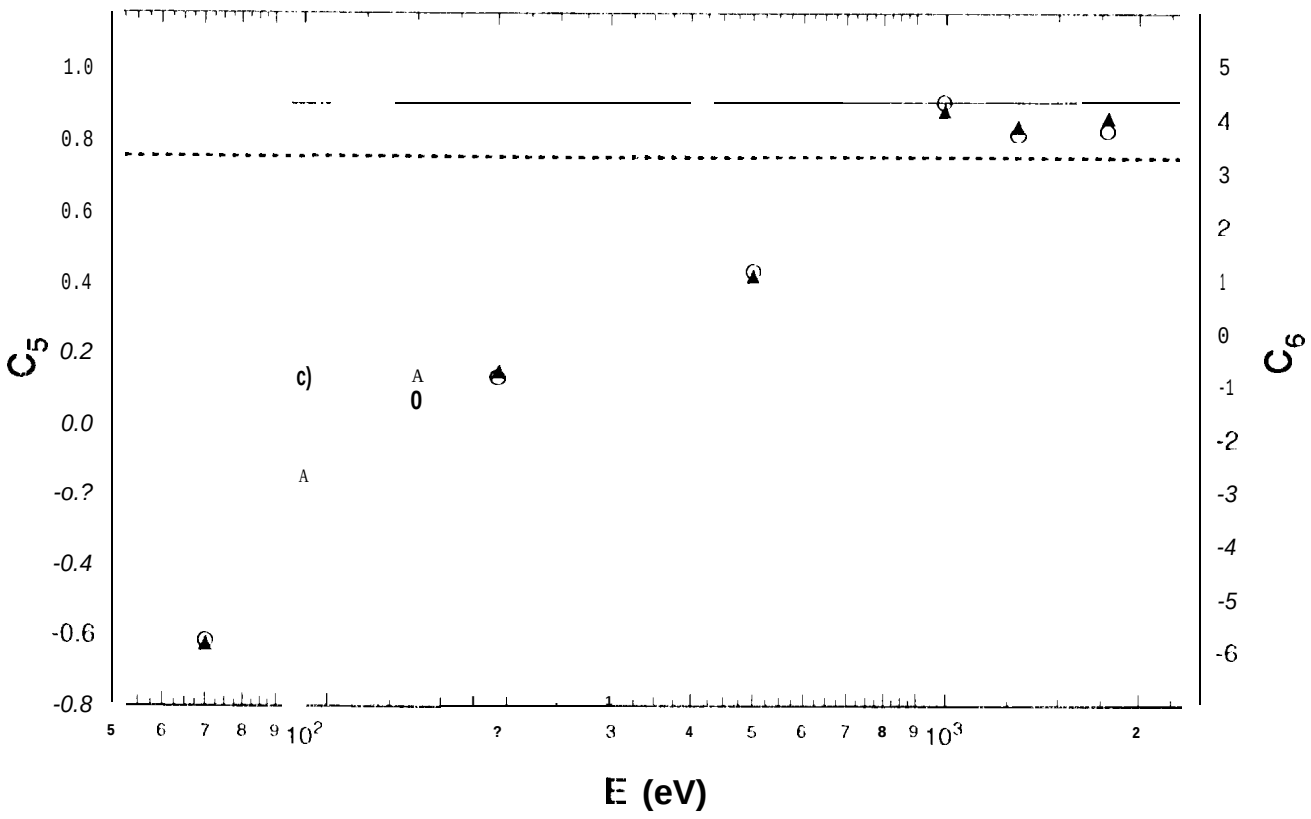

FIG. 13. The variation of the 1st (C_5, open circles) and 2nd (C_6, triangles) order coefficients of the analytic function Eq. 10, fitted to the Ref. [20] CCC calculations truncated at the energies indicated on the abscissa. In the ideal case the coefficients should be invariant on this plot. The Born values of C_5 and C_6 are indicated by the solid and dashed lines, respectively.

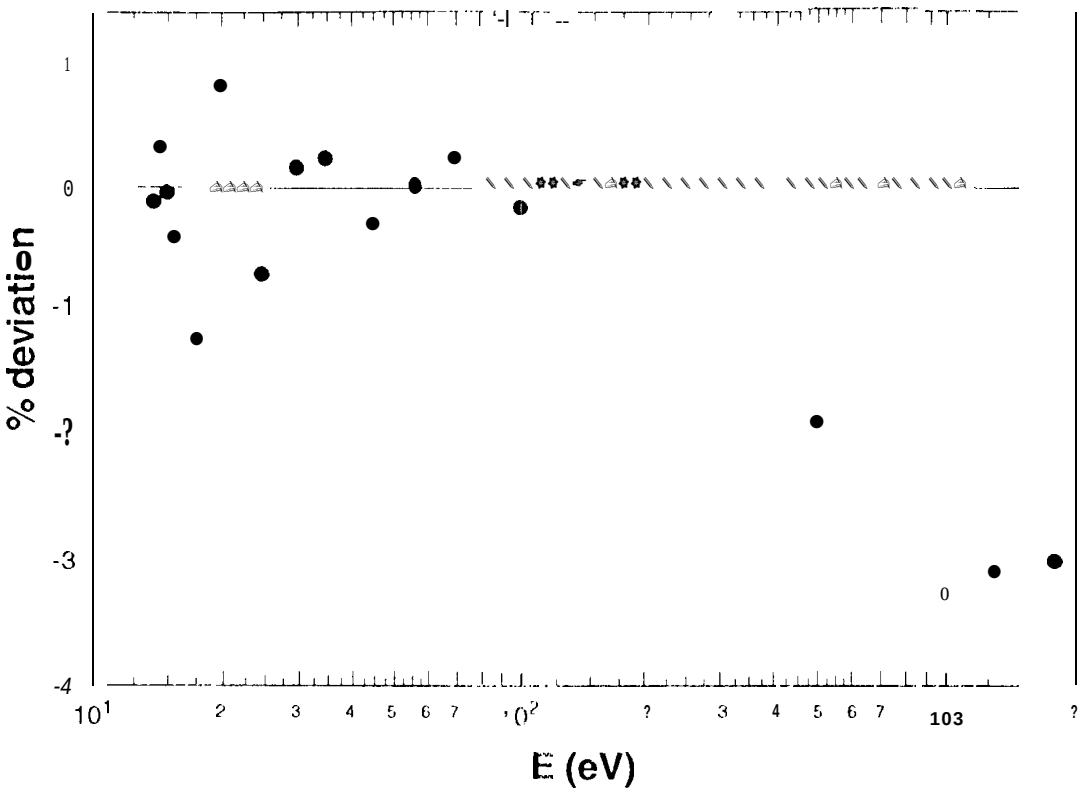

FIG. 14. Deviation of analytic model, Eq. 10, from Bray CCC (Ref. [20]) calculations of the H (1s 2p) collision strength. The analytic model fit was limited to 200 eV in the Bray data. The plotted points are the percentage deviation calculated after subtracting the CCC calculations from the model values.

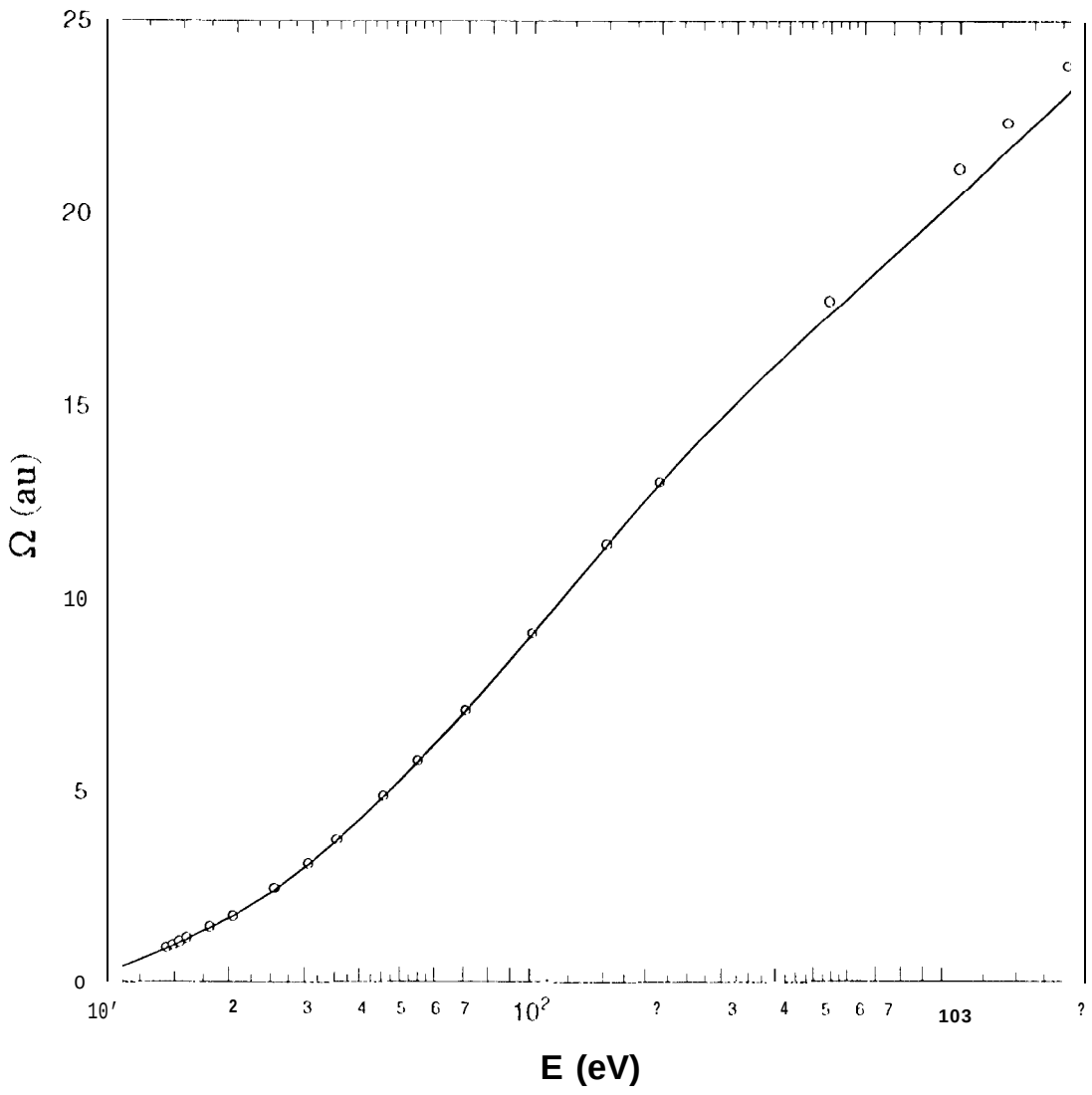

FIG. 15. Recommended **11 (1s** 2p) analytic electron collision strength (see text) derived from the Bray[20] CCC **calculations** (solid line) compared to the theoretical CCC values of Bray [20] (open circles).

TABLES

TABLE Collision Strength Coefficients

Coefficient[a]	orn[b]	Experiment[c]	Theory[d]	Theory[e]	Cascade[f]
C_0	···	- 6.0221	···	- 3.6969	- 3.3707
C_1	··	- 8.6381	- 10.387	- 7.1941	3.7832
C_2	··	15.988	30.798	3.8606	6.8398
C_3	···	- 16.566	- 53.092	- 4.0690	21.950
C_4		···	38.965	···	···
C_5	0.8988	0.29151	0.12536	- 1.0997	0.36692
C_6	3.3358	4.161	- 0.73427	11.159	0.41985
C_7	4.447	4.4475	4.4470	4.7500	0.055239
C_8	···	0.060256	0.17990	0.1349	1.1220

[a] See text, Eq 4a, 10

[b] H (1s 2p); Born approximation, Eq. 9a

[c] H (1s 2p); Present work

[d] H (1s 2p); Analysis of Ref. [20] calculations to 200 eV, fiixing the value of C_7 by the value of f_{ij}

[e] H (1s 2p); Analysis of Ref. [20] calculations to 2 keV

[f] H (1s nℓ) → H (2p + nℓ); Calculated cascade into the H(2p) state (Ref. [31]), see text

TABLE II II (1s - 2p) Measured Electron Impact Cross section(au)

E (eV)	$Q_{1s2p}(E)^a$	$Q_{1s2p}(E)^b$	E (eV)	$Q_{1s2p}(E)^a$	$Q_{1s2p}(E)^b$	E (eV)	$Q_{1s2p}(E)^a$	$Q_{1s2p}(E)^b$
1.134+01	3.494-01	3.662-01	9.706+01	6.038-01	6.328-01	1.828+02	4.499-01	4.715-01
1.329+01	3.847-01	4.032-01	9.901+01	5.759-01	6.035-01	1.847+02	4.178-01	4.378- 01
1.524+01	4.485-01	4.700-01	1.010+02	5.888-01	6.170-01	1.867+02	4.192-01	4.393- 01
1.719+01	4.961-01	5.199-01	1.029+02	5.927-01	6.211-01	1.886+02	4.153-01	4.352- 01
1.914+01	5.683-01	5.956 01	1.049+02	5.663 01	5.934-01	1.906+02	4.153-01	4.352- 01
2.109+01	5.805-01	6.084-01	1.068+02	5.694-01	5.967-01	1.925+02	4.122-01	4.319- 01
2.303+01	5.804-01	6.083-01	1.088+02	5.725-01	6.000-01	1.964+02	4.174-01	4.374- 01
2.498+01	6.536-01	6.850-01	1.107+02	5.399 01	5.658 01	1.984+02	3.980-01	4.171- 01
2.693+01	6.192-01	6.489-01	1.126+02	5.550 01	5.817-01	2.000+02	3.915-01	4.103 01
2.888+01	6.750-01	7.074-01	1.146+02	5.531-01	5.797-01	2.600+02	3.390-01	3.552- 01
3.083+01	6.944-01	7.277-01	1.165+02	5.441-01	5.702-01	3.000+02	3.206-01	3.360- 01
3.277+01	6.477-01	6.788 01	1.185+02	5.463 01	5.725-01	3.500+02	2.956-01	3.098- 01
3.472+01	6.670-01	6.990-01	1.204+02	5.317-01	5.572-01	4.000+02	2.666-01	2.794- 01
3.667+01	6.836-01	7.164-01	1.224+02	5.152-01	5.399 01	4.500+02	2.505-01	2.625- 01
3.862+01	6.924-01	7.256-01	1.243+02	5.319 01	5.575-01	5.000+02	2.328-01	2.440- 01
4.057+01	7.022-01	7.359-01	1.263+02	5.201-01	5.450 01	5.500+02	2.168-01	2.272- 01
4.251+01	6.668-01	6.988-01	1.282+02	5.258 01	5.510 01	6.000+02	2.014 01	2.111- 01
4.446+01	6.724-01	7.047-01	1.302+02	5.301-01	5.556-01	6.500+02	1.912-01	2.003- 01
4.641+01	6.863-01	7.193-01	1.321+02	4.937-01	5.174-01	7.000+02	1.786-01	1.872- 01
4.836+01	7.029-01	7.367-01	1.341+02	5.142-01	5.388-01	7.500+02	1.708-01	1.790- 01
5.031+01	6.875-01	7.205-01	1.360+02	5.378 01	5.636-01	8.000+02	1.624-01	1.701- 01
5.225+01	6.846-01	7.175-01	1.380+02	4.964-01	5.202-01	8.500+02	1.568-01	1.644- 01
5.420+01	6.713-01	7.035-01	1.399+02	5.119-01	5.364-01	9.000+02	1.480-01	1.551- 01
5.615+01	6.768-01	7.093-01	1.419+02	5.014-01	5.255-01	9.500+02	1.430-01	1.498- 01
5.810+01	6.895-01	7.226-01	1.438+02	4.913 01	5.148-01	1.000+03	1.389-01	1.455- 01
6.005+01	6.544-01	6.858-01	1.458+02	5.033-01	5.275-01	1.050+03	1.342-01	1.407- 01
6.200+01	6.664-01	6.984-01	1.477+02	4.786 01	5.016-01	1.100+03	1.268-01	1.329- 01
6.394+01	6.936-01	7.269-01	1.497+02	4.985 01	5.224-01	1.150+03	1.230-01	1.289 01
6.589+01	6.265-01	6.566-01	1.516+02	4.592-01	4.813-01	1.200+03	1.172-01	1.228 01
6.784+01	6.444-01	6.753-01	1.536+02	4.861-01	5.095-01	1.250+03	1.165-01	1.221- 01
6.979+01	6.591-01	6.908-01	1.555+02	4.735-01	4.962-01	1.300+03	1.115-01	1.169- 01
7.174+01	6.244-01	6.544-01	1.575+02	4.735-01	4.962-01	1.350+03	1.078-01	1.130- 01
7.368+01	6.488-01	6.799 01	1.594+02	4.534-01	4.752-01	1.400+03	1.053 01	1.104- 01
7.563+01	6.414-01	6.722-01	1.614+02	4.924-01	5.160-01	1.450+03	1.027-01	1.076- 01
7.758+01	6.308 01	6.611-01	1.633+02	4.425 01	4.637-01	1.500+03	9.920 02	1.040 01
7.953+01	6.282-01	6.584-01	1.652+02	4.795 01	5.025-01	1.550+03	9.820 02	1.029- 01
8.148+01	6.104-01	6.397-01	1.672+02	4.716 01	4.942-01	1.600+03	9.506-02	9.962- 02
8.342+01	6.015-01	6.304-01	1.691+02	4.542-01	4.760-01	1.650+03	9.220-02	9.662- 02
8.537+01	6.188-01	6.485-01	1.711+02	4.496 01	4.712-01	1.700+03	9.049-02	9.484- 02
8.732+01	5.943-01	6.228-01	1.730+02	4.286 01	4.492-01	1.750+03	8.849-02	9.274- 02
8.927+01	5.969-01	6.255-01	1.750+02	4.394-01	4.604-01	1.800+03	8.598-02	9.011- 02
9.122+01	5.894-01	6.176-01	1.769+02	4.419-01	4.631-01	...	...	...
9.316+01	5.936-01	6.221-01	1.789+02	4.355-01	4.564-01	...	...	
9.511+01	5.767-01	6.044-01	1.808+02	4.223 01	4.426-01	...	...	

[a] Present measured cross section, corrected and scaled using analytic fit, as discussed in text.

[b] Present measured cross section, normalized using Bethe-Fano plot as described by Ref. [1] These values are the upper limit of the true cross section.

[c] Read as $.134 \times 10$

TABLE III.H (1s 2p): Comparison of Electron Impact Cross Sections(au)

E (eV)	$Q_{1s2p}(E)$				
1.40+01[a]	4.28E-01[b]	4.26 01[f]			4.42-01[f]
1.45+01	4.47-01	4.48E-01			4.62-(11
1.50+01	4.67-01	4.67E-01	8.34-01[d]		4.7(1-01
1.56+01	4.89-01	4.87E-01			4.96 (11
1.76+01	5.48 01	5.41E-01			5.38 01
2.0(1-1 01	5.85-01	5.89E-01	8.78-01		5.73-01
2.50+01	6.62-01	6.57E-01	8.99-01		6.21-(11
3.00+01	6.98 01	6.99-01	...		6.51-01
3.50+01	7.21-(11	7.23 01			6.70 01
4.50+(11	7.4001	7.38 01			6.83-01
5.44+01	7.29 01	7.29 01	8.46 01		6.78-01
7.00+01	6.92-01	6.94-01	7.81 01		6.51-01
1.00+02	6.20-01	6.19 01	6.76 (11	6.01-01[e]	5.81-01
1.50+02	5.1801	5.18-01	5.46 01		4.80 01
2.(1(1-! 02	4.43-(11	4.44 01	4.59 (a 1	4.14-01	4.09-01
3.00+02		3,42-01		3.02-01	3.20 01
1.(J(l-l 02		2.79 01		2.60-01"	2.67-01
5.00+02	2,42.01	2.37-01	2.42-01		2.30-01
9.99+02	1..11 01	1.40 01	1.43(11		1.38 01
1.30+03	1.17-01	1.1301			1.12-(11
1.80+03	9.01-02	8.74-02			8.61-02
2.0(1-1 03		8.02-02			7.9-(I2
3.00+03		5.76 02			5.68-02
4.00+03		4.54-02			4.47-(I2
5,(1( )-l 03		3.76-02			3.71 -02
6.00+03		3.23 02			3.19-02
7.00+(1'1		2.8302			2.80-02
8.00+ 03		2.53-02			2.5(1-(12
9.0( )-I 03		2.29-02			2.26-[12
1.00-104		2.09 0'2			2.06 (I2

[a] Read as 1.4 $\times 10^1$

[b] CCC method; Ref. [20].

[c] Analytic fit to Ref. [20] data to 200 eV, Eq. 10.

[d] DWBA2 method; Ref. [17].

[e] UEBS method; Ref. [25].

[f] Analytic fit to present experimental data; see text.

TABLE V. (1s - 2p) Selected Electron Impact Cross Sections(au)

E (eV)	$Q_{1s2p}(E)$		
11.0	0.192[a]	...	0.212[e]
13.4	0.413	0.42[b]	0.332
16.0	0.506	0.50	0.424
18.5	0.553	0.55	0.473
23.5	0.609	0.65	0.570
28.5	0.643	0.70	0.624
38.6	0.678	0.72	0.658
48.6	0.683	0.72	0.650
54.4	0.678	0.888[c]	...
68.6	0.654	0.68[b]	0.623
88.7	0.608	0.64	0.578
118.8	0.540	0.56	0.505
148.9	0.482	0.52	0.466
200.0	0.409	0.45	0.409
1000.0	0.138	0.135[d]	...
1200.0	0.119	0.126	...
1400.0	0.105	0.109	...
1600.0	0.095	0.099	...
2000.0	0.079	0.086	...

[a]Analytic fit to present experiment.

[b]van Wyngaarden and Walters [8] reanalysis of ref. [1] experiment; see text.

[c]Williams [2].

[d]Schartner [50]

[e]Present reanalysis of Ref. [1] experiment; see text.

TABLE V. Recommended electron impact 11 ( ] s 2p) ('1'oss section

E (eV)	Q_{1s2p}(E)	E (eV)	Q_{1s2p}(E)	E (eV)	Q_{1s2p}(E)
1.50+01[a]	4.667-0][b]	2.65+01	6.720-01	1.00+02	6.186-01
1.52+01	4.737-01	2.70+01	6.764-01	1.10+02	5.959-01
1.54+01	4.801-01	2.80+01	6.846-01	1.20+02	5.747-01
1.56+01	4.868 01	2.90+0]	6.920-01	1.30+02	5.548 01
1.58+01	4.931-01	3.00+01	6.987-0]	1.40+02	5.360-01
1.60+01	4.991-01	3.10+01	7.04801	1.50+02	5.184-01
1.62+01	5.050 01	3.20+01	7.10-01	1.60+02	5.018 01
1.64+01	5.1() 6-(11	3.30+01	7.149 01	1.70+0'?	4.86((11
1.66+01	5.161-01	3.4(I(01	7.1$12-01	1.80+02	4,7' 11-(11
1.68+ 01	5.21,1 -[)1	3.50+01	7.229-0]	1.90+02	4.57[)- (11
1.70+01	5.266 01	3.60-[0]	7.261-O]	2.00-102	4.436-01
1.72+01	5.316 01	3.70-101	7.2 S$1.01	2.50+02	3.864 (11
1.74+01	5.365-01	3.80+01	7,312-01	3.00+02	3,421-01
1.76+01	5.412-(11	3.90+01	7.332-01	3.50 I 02	3.072.(1]
1.78+01	5.458 01	4.00 + 01	7.347-01	4.00 +02	2.792- (II
1.80+01	5.503-01	4.10+01	7.360-01	4.50-I0'2	2.562-01
1.92+0]	5.750 01	4.20+01	7.369-01	5.00+02	2.370 01
1.94+01	5.788-01	4.30+01	7.375-01	5.50+02	2.207-(,1
1.96+01	5.825-01	4.40+01	7.378 01	6.00+02	2.067- (,1
1.98+01	5.861-01	4.50+01	7.378 01	7.00+02	1.83901
2.00+01	5.896 01	4.60+01	7.377-01	8.00+02	1.66001
2,0:1-101	5.980 01	4.'70 I 01	7'.372-01	9.00+02	1.515-01
2.10+01	6.060-01	4.80+01	7.366-01	1.00+03	1.395-01
2.15+01	(i,]3601	4.90+01	7.358-01	1.20-1 03	1.209-01
2.20+01	6.209-01	5.00+01	7.348-01	1.40-103	1.06() -01
2.25+01	6.277-01	5.44+01	7.287-01	1.60+ 03	9.610-02
2.30+01	6.342-01	6.00+01	7.179-01	1.80+ 03	S.74(1.02
2.35+01	6.404 01	6.50-101	7.(164-O]	2.00+03	8.02602
2.40-$01	6.464-01	7.00+01	6.940-01	2.50+03	6.691-02
2.45+01	6.520.01	7.50+01	6.81 1-01	3.00+ 03	5.760-02
2.50+01	6..574.01	8.0(1-1 01	6.682-01	3.50-103	5.07(1-02
2.55+01	6.625-01	8.50101	6.554-01	4.00+03	4. S38-02
2.60+01	(3.674-01	9.0()-(01	6.428-01	4.50+03	4.113-02
		9.50+ 01	6.305-01	5,()()+ 03	3.765-02

[a]Read as 1.50×10^{1}

[b]Recommended cross section (au) from analytic fit to to Ref. [20]. See Table I, ('01 4, for analytic coefficients